Coverage Performance in MIMO-ZFBF Dense HetNets with Multiplexing and LOS/NLOS Path-Loss Attenuation

Mohammad G. Khoshkholgh, *Memeber, IEEE*, Keivan Navaie, *Senior Memeber, IEEE*, Kang G. Shin, *Life Fellow, IEEE*, Victor C. M. Leung, *Fellow, IEEE*

Abstract—The performance of multiple-input multiple-output (MIMO) multiplexing heterogenous cellular networks are often analyzed using a single-exponent path-loss model. Thus, the effect of the expected line-of-sight (LOS) propagation in densified settings is unaccounted for, leading to inaccurate performance evaluation and/or inefficient system design. This is due to the complexity of LOS/non-LOS models in the context of MIMO communications. We address this issue by developing an analytical framework based on stochastic geometry to evaluate the coverage performance. We focus on the zero-forcing beamforming where the maximum signal-to-interference ratio is used for cell association. We analytically derive the coverage. We then investigate the cross-stream interference correlation, and develop two approximations of the coverage: Alzer Approximation (A-A) and Gamma Approximation (G-A). The former is often used in the single antenna and single-stream MIMO. We extend A-A to a MIMO multiplexing system and evaluate its utility. We show that the inverse interference is well-fitted by a Gamma random variable, where its parameters are directly related to the system parameters. The accuracy and robustness of G-A is higher than that of A-A. We observe that depending on the multiplexing gain, it is possible to attain the best coverage probability by proper densification.

Index Terms—Area spectral efficiency, coverage probability, densification, heterogenous cellular networks (HetNets), LOS/NLOS path-loss model, multiple-input multiple-output (MIMO), multiplexing, numerical complexity, Poisson Point Process (PPP), stochastic geometry, zero-forcing beamforming (ZFBF).

1 Introduction

Densification of heterogenous cellular networks (HetNets) as well as air interface technology based on multiple-input multiple-output (MIMO) are viable ways to address the rapid and substantial growth of mobile data demand. In fact, these two technologies have been integral parts of the air interface technology in 5G and beyond [2], [3], thanks to a set of encouraging analytical results in [4], [5], [6], [7] demonstrating a nearly proportional growth of the area spectral efficiency (ASE) in HetNets by steadily increasing the number of BSs per unit area (*densification*) without deteriorating the coverage probability (*scale invariance*). These analytical results were developed by leveraging tools of stochastic geometry (e.g., [8], [9], [10], and validated with empirical studies, e.g., [11], [12].

- *The paper received March 27, 2018, revised February 20, 2019 and May 17, 2019. The paper is accepted June 5, 2019. An earlier version of this work was presented in IEEE VTC-Fall, 2017, Toronto [1]. The corresponding author is V. C. M. Leung.*
- *M. G. Khoshkholgh (e-mail: m.g.khoshkholgh@gmail.com) is with the Department of Electrical and Computer Engineering, the University of British Columbia, Vancouver, BC, Canada V6T 1Z4; V. C. M. Leung is with the College of Computer Science and Software Engineering, Shenzhen University, Shenzhen 518060, China, and also with the Department of Electrical and Computer Engineering, The University of British Columbia, Vancouver, BC V6T 1Z4, Canada (e-mail:,vleung@ieee.org); K. Navaie (e-mail: k.navaie@lancaster.ac.uk) is with the School of Computing and Communications, Lancaster University, Lancaster, United Kingdom LA1 4WA; K. G. Shin (e-mail: kgshin@umich.edu) is with the Department of Electrical Engineering and Computer Science, University of Michigan, Ann Arbor, MI 48109-2121, U.S.A.*
- *This work was supported in part by the National Natural Science Foundation of China under Grant 61671088, in part by the Vanier Canada Graduate Scholarship, in part by the National Engineering Laboratory for Big Data System Computing Technology at Shenzhen University, China, and in part by the Natural Sciences and Engineering Research Council of Canada.*

The scale invariance property of HetNets, however, depends heavily on the standard path-loss model (SPLM) $L(\|x\|) = \|x\|^{-\alpha}$, where $\|x\|$ is the Euclidean distance between the source and the destination, and $2 < \alpha < 8$ is the path-loss exponent. Nevertheless, SPLM has intrinsic disadvantages, such as singularity—where the received power may increase significantly as $\|x\| \rightarrow 0$, which results from ultra densification [13]. It is shown in [13], [14] that in contrast to the analysis based on SPLM, the coverage probability under a bounded path-loss function, e.g., $L(\|x\|) = \|x+1\|^{-\alpha}$, is decreased by increasing the density of base stations (BSs). A similar conclusion was drawn in [15], where the coverage probability in a double-slope path-loss environment was shown to decrease significantly due to densification. Such conclusions are in contrast with those of made in [4], [5], [6], [7] based on SPLM. This is because SPLM fails to model the propagation in mobile systems such as small cells, where a combination of line-of-sight (LOS), and non-LOS (NLOS) links are involved with the inside/outside of buildings.

The need for an inclusive path-loss attenuation model which is able to characterize propagation in the cellular networks in various environments is also recognized by the 3GPP. In 3GPP TR36.814, Release 9 [16], a practical path-loss model is described as the one that can distinguish between Line of Sight (LOS), and non-LOS (NLOS) links. Such models will henceforth be referred to as *LOS/NLOS models*. Adopting a 3GPP LOS/NLOS path-loss model [16], scale invariancy is shown to be not preserved in ultra-dense cellular networks [17], [18]. This is due to the fact that closer BSs show higher tendency to exhibit the LOS effect—with a smaller path-loss exponent—while farther BSs are most likely to demonstrate NLOS path-loss attenuation. Therefore, the inter-cell interference (ICI) eventually dominates the received signal power.

Hence, the analytical results obtained based on the SPLM are only reliable in cases where the network is, at most, moderately densified. In such a case, signals from most of the BSs, both serving and interfering, close to the user equipment (UE) are propagating through a NLOS link. However, this might not be a valid assumption for heavily densified HetNets [19], [20], where it is most likely for a UE to have LOS signals, both from the interferers and the serving BS. Therefore, there is an urgent need to re-visit the performance evaluation of HetNets while considering the LOS/NLOS path-loss model .

Several models have been proposed to characterize the path-loss attenuation in dense HetNets. A multi-ball path-loss model was proposed, and then the spectral efficiency and coverage performance of a single-tier cellular network was investigated in [21]. The analysis was then validated using empirical data collected in various cities [21].

The effect of NLOS link propagation on the outage probability was also studied in [22], where the authors constructed a new analytical path-loss model, formulating the probability of realizing the LOS propagation with distance, average size and density of the buildings per area. The Boolean blockage model [22] was further utilized in [23] to incorporate the effect of the size and density of buildings as well as the wall penetration on the performance evaluation of a two-tier HetNet. Their work distinguishes between indoor small cell BSs and outdoor Macro BSs, and also takes into account the signal propagation characteristics of LOS, NLOS, and blocked modes.

Similarly, the area spectral efficiency (ASE) is closely related to the path-loss model. The authors of [24] studied the fundamental limits of ultra-dense networks according to fading distribution, shadowing, and multi-slope path-loss attenuation. Adopting the tools of stochastic geometry along with the extreme value theory, the authors of [24] obtained scaling laws governing the downlink SINR, coverage probability, and spectral efficiency. It is also shown in [25] that the spectral efficiency may be reduced substantially by densification if the LOS path-loss exponent becomes very small. The same behavior was reported for the uplink in an ultra-dense single-tier cellular network with multi-slope path-loss attenuation [26].

The main focus in the above-mentioned studies, e.g., [13], [14], [15], however, is on single-tier networks with SISO-based air interface. Despite its relevance and importance, to the best of our knowledge, the coverage performance of MIMO multiplexing in a multi-tier HetNet with LOS/NLOS path-loss attenuation has not been fully investigated. An instance for practical applications of such systems is in sub-6 GHz spectrum [2], [16].

The importance of an accurate path-loss model is also witnessed in the emerging literature. For instance, the authors of [27] demonstrated the feasibility of MIMO communications in wireless energy harvesting applications, and highlighted further the crucial role of LOS component in enhancing the rate of harvesting energy and decoding probability. Moreover, [28] studied the coverage probability and spectral efficiency of multi-tier mmWave communications for both noise- and interference-limited scenarios, in the presence of practical beamforming alignment error, LOS/NLOS and blockage model. The results were then extended in [29] to investigate the potential of cellular systems for simultaneous information and wireless power transfer. The antenna's directionality was shown instrumental to (partially) cancel out the severe effect of LOS interference as a result of network densification. Understanding the impact of LOS/NLOS on the coverage and ASE of MIMO multiplexing systems, however, has not yet been considered.

We consider a link-level coverage performance analysis in which successful reception of all data steams is considered as a successful transmission. This is different from the conventional approach, *stream-level* analysis, which defines a successful transmission as the successful reception of a single data stream. In fact, our previous results [30], [31], [32], [33] indicate that the coverage performance of MIMO multiplexing HetNets with SPLM is best represented by their *link-level* analysis. Thus, part of this paper could be considered as an extension of our previous results to systems with LOS/NLOS path-loss attenuation.

The coverage probability as a function of different system parameters is often incorporated in adaptive HetNet resource allocations, as well as system design problems [34], [35], [36]. Therefore, a quick and accurate estimation of the coverage probability is important to the optimization of the system operating parameters on-the-go. Adopting the LOS/NLOS propagation model makes it challenging to analyze coverage performance in such systems. In this paper, we derive closed-form analytical results and then propose quick and accurate approximations.

We leverage stochastic geometry to obtain a closed-form expression for the coverage probability. Calculating the coverage probability based on derived closed-form, however, requires substantial numerical calculations. The complexity of the problem has its root in the intrinsic correlation in the inter-cell interference (ICI) across streams. This is due to the packed geometry of MIMO dense networks in which the interferers to each data stream are not independent. To address this issue, we analytically investigate the cross-stream ICI correlation in a MIMO HetNet setting with multiplexing. Our analysis indicates a very high correlation in ICI across stream. This justifies the construction of 'full-correlation' (FC) approximation, where the ICI across all streams on a given communication link is considered fully correlated.

The FC assumption is then used in our proposed Alzer Approximation (A-A) of the coverage probability. We further propose a new approximation based on a novel way of modeling the inverse ICI using a fitted Gamma distribution, i.e., Gamma Approximation (G-A). We then obtain the parameters of the fitted Gamma distribution as functions of main system and path-loss parameters. This approximation is presented for the first time.

Both A-A and G-A need significantly lower numerical computations than that of the originally obtained closed-form. Our extensive simulation and numerical results indicate that the G-A outperforms the A-A in terms of accuracy while its corresponding computational complexity is slightly higher. Our simulation results also reveal that G-A demonstrates a higher level of robustness to a wide range of system parameters, including density of BSs, multiplexing gains, and LOS path-loss exponent. As its practical importance, the proposed G-A, unlike A-A, pinpoints the optimal density for which the best coverage performance is achieved. Our results suggest that G-A is a much better choice than that of the A-A for MIMO communications (including mmWave communications), and also single-antenna system under Nakagami fading.

We further utilize the results in this paper to approximate the coverage performance of diversity-only MIMO system in HetNet systems with *homogeneous/nonhomogeneous* SPLM. Our results show that compared to multiplexing systems, diversity-only systems provide a higher coverage performance without degrading ASE. Interestingly, in a 2-tier HetNet, when densification in Tier 2 improves the coverage probability, it can counterproductively acts in an environment with LOS/NLOS path-loss attenuation.

Our numerical studies further provide quantitative insights into the impacts of densification, multiplexing, and the propagation environment on the coverage probability and ASE. Our results also show that by careful selection of BS density in each tier, one can exploit the existence of the LOS propagation to improve ASE. In such a setting, the ASE gain is higher for cases with smaller LOS path-loss exponents.

Note that the focus of the earlier conference version [1] of this paper was on a single-tier network, where only a specific LOS/NLOS model was considered. Here the results in [1] are extended to a K-tier HetNet with the generic LOS/NLOS, where we also develop A-A and G-A. Furthermore, this paper incorporates the cross-stream ICI correlation, which was absent in [1].

The rest of this paper is organized as follows. Section 2 reviews the literature of performance evaluation of MIMO communications under the stochastic geometry. Section 3 presents the system model which is followed by the definition of the the coverage probability in multiplexing systems in Section 4. Section 5 considers ICI correlation, introduces FC assumption, and develops the A-A and G-A methods. Section 6 utilizes our analytical results to evaluate the coverage performance in MIMO diversity only systems, ZFBF with nonhomogenous and homogenous SPLM, and systems with available CSI at the transmitter (CSIT). Numerical and simulation results are then presented in Section 7, followed by conclusions in Section 8.

2 Related Work

The main focus of this paper is on the MIMO multiplexing systems where stochastic geometry tools are used in our analysis. Using SPLM assumption, the authors of [37] investigate the coverage probability of several prominent MIMO techniques in ad hoc networks. Furthermore, in [38] the impact of inaccurate channel state information on the coverage probability is investigated in a clustered MIMO ad hoc network. It is shown in [38] that in interference-limited scenarios using single-user MIMO communications can improve the coverage performance. Coverage performance and ASE of multiple-user spatial-division multiple access (SDMA) in multiple-input single-output (MISO) HetNets is also investigated in [7], [39] and [40] for cases where cell association (CA) is based on *range expansion*, i.e., UEs are associated with BSs with the smallest path-loss scaled by a range extension parameter. A novel technique was developed in [41] that can be used for the evaluation of functionals of Poisson point processes and the SIR distribution of wireless systems under Nakagami fading. Further, a moment-generating method for approximating the SIR distribution of SISO systems under Nakagami fading was developed in [42]. The authors of [43] and [44] focused on maximum ratio combining (MRC) and optimal combining in downlink and uplink of cellular networks, respectively. The Gil-Pelaez inversion theorem [45] is found instrumental in analyzing the symbol error probability (SEP) of MIMO multiplexing systems [46].

An equivalent-in-distribution (EiD) technique was suggested in [47] to understand the SEP of MIMO communications. A unified method for studying the SEP in MIMO communications was proposed in [48] by adopting the EiD method. Moreover, the impact of interference-driven correlation on receiver arrays in ad-hoc network as well as the downlink of a single-tier cellular network was investigated in [49] and [50]. The authors of [51], [52], [53] demonstrated the importance of theoretical results developed in [7], [40], [42] for the optimization of MIMO ellular systems. For instance, in [52], the coverage probability, spectral efficiency, and load balancing in MIMO systems were considered. Further, [51] optimized ASE and energy-efficiency in uplink/downlink multi-user MIMO system. For managing inter-cell interference, [54] investigated the coupled optimized offloading and coordinated MIMO communications. Energy-efficiency of MIMO downlink was also the subject of [55] the authors which attempted to highlight the significance of beamforming schemes.

Although significant in their own rights, all of the above efforts rely on the restricted path-loss model of SPLM and often consider single-stream MIMO communication. For a more practical path-loss model, researchers often adopted Alzer's Theorem to derive the coverage probability of a SISO system under Nakagami fading and single-stream multi-user MIMO systems [17], [23], [56], [57]. The coverage probability of a heterogenous device-to-device mmWave systems was studied in [58], confirming the utility and accuracy of the Alzer method. The authors further introduced a mixed inverse-gamma log-normal distribution to approximate the interference distribution under LOS/NLOS path-loss model.

In this paper we extend the Alzer method to the case of MIMO multiplexing systems to investigate its accuracy and use as a benchmark for comparison with G-A approximation. For MIMO-ZFBF and under LOS/NLOS path-loss model in [59], [60], the transmission delay of a single-tier wireless ad hoc network was investigated. The importance of LOS/NLOS path-loss model for achievable optimization of the network was highlighted. Further, importance of spatially-coded MIMO configuration, packet retransmission, and advanced hybrid repeat request protocols were demonstrated. However, their analyses are applicable only to single-tier ad hoc networks, and may not be extensible to the multi-tier cellular systems under max-SIR CA rule.

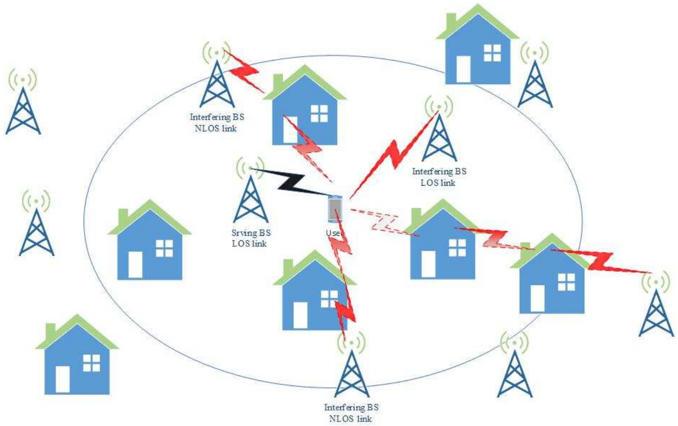

Fig. 1. A schematic of the system model for $K = 1$. A BS located closer to the origin has a higher chance of LOS propagation. Because of the NLOS path-loss, the signals received from farther BSs are substantially weaker. Nevertheless, the typical UE can still be associated with a BS in NLOS mode due to, for example, fast fading fluctuations.

3 System Model

We investigate the downlink communication in a multi-tier cellular network. The network is comprised of $K \geq 1$ tiers of randomly located base stations (BSs), where the BSs of tier i, $i \in \mathcal{K} = \{1, \ldots, K\}$, are spatially distributed according to a homogenous Poisson point process (PPP), Φ_i, with spatial density, λ_i (the number of BSs per unit area), $\lambda_i \geq 0$. PPPs, $\Phi_i, \Phi_j, \forall i, j \in \mathcal{K}, i \neq j$ are mutually independent. A HetNet consists of Φ_i, $i \in \mathcal{K}$, i.e., $\{\Phi_i\}_{\forall i}$, is referred to as Φ.

UEs are randomly positioned across the network and form a PPP, Φ_U, independent of Φ, with given density, λ_U. According to Slivnayak's Theorem [61], [62] and due to the stationarity of the point processes, the spatial performance of the network can be obtained from the perspective of a typical UE positioned at the origin. We also assume that UEs are equipped with N^r antennas.

Tier i is fully characterized by the corresponding spatial density of BSs, λ_i, their transmission power, P_i, the minimum required received SIR for the UEs in Tier i, $\beta_i \geq 1$, the number of the transmit antennas at the BSs, N_i^t, and the number of scheduled streams $S_i \leq \min\{N_i^t, N^r\}$ also referred to as *multiplexing gain* [30], [63], [64]. Fig. 1 shows a schematic model of the network for $K = 1$.

3.1 Generic LOS/NLOS Path-Loss Model

A block fading wireless channel is considered, where at the beginning of each time slot, an independent realization of the fading is generated and stays fixed throughout that time slot. The typical UE is associated with BS x_i, transmitting S_i data streams. The received signal, $\boldsymbol{y}_{x_i} \in \mathbb{C}^{N^r \times 1}$, is

$$\boldsymbol{y}_{x_i} = \sqrt{L_i(\|x_i\|)}\boldsymbol{H}_{x_i}\boldsymbol{s}_{x_i} + \sum_{j \in \mathcal{K}} \sum_{x_j \in \Phi_j \setminus x_i} \sqrt{L_j(\|x_j\|)}\boldsymbol{H}_{x_j}\boldsymbol{s}_{x_j}, \tag{1}$$

where $\forall x_i, i \in \mathcal{K}$, $\boldsymbol{s}_{x_i} = [s_{x_i,1} \ldots s_{x_i,S_i}]^T \in \mathbb{C}^{S_i \times 1}$, $s_{x_i,l_i} \sim \mathcal{CN}(0, P_i/S_i)$ is the transmitted signal corresponding to stream l_i in Tier i, $\boldsymbol{H}_{x_i} \in \mathbb{C}^{N^r \times S_i}$ is the fading channel matrix between BS x_i and the typical UE, with entries independently drawn from $\mathcal{CN}(0, 1)$. Transmitted signals across different BSs are also assumed to be mutually independent, and also independent of the channel matrices. In (1), $L_i(\|x_i\|)$ is a generic distance-dependent path-loss function, where $\|x_i\|$ is the Euclidean distance between BS x_i and the origin, which is random.

As shown in Fig. 1, a BS experiences LOS or NLOS propagation, depending on its relative distance to the UE, density of buildings, type of the clutter, etc. To model LOS/NLOS pathloss, we adopt the path-loss model recommended in the 3rd Generation Partnership Project (3GPP) [16], [17], [18], where the path-loss attenuation in Tier i is

$$L_i(\|x_i\|) = \begin{cases} L_{\mathrm{L}}^i(\|x_i\|) & \text{with probability of } p_{\mathrm{L}}^i(\|x_i\|), \\ L_{\mathrm{N}}^i(\|x_i\|) & \text{with probability of } p_{\mathrm{N}}^i(\|x_i\|). \end{cases} \tag{2}$$

For $n_i \in \{\mathrm{L}, \mathrm{N}\}$, function $L_{n_i}^i(\|x_i\|)$ can adopt any feasible path-loss function, e.g., $L_{n_i}^i(\|x_i\|) = \phi_{n_i}^i \|x_i\|^{-\alpha_{n_i}^i}$, $L_{n_i}^i(\|x_i\|) = \phi_{n_i}^i (1 + \|x_i\|)^{-\alpha_{n_i}^i}$, or $L_{n_i}^i(\|x_i\|) = \phi_{n_i}^i \max\{1, \|x_i\|^{-\alpha_{n_i}^i}\}$, where α_{L}^i (α_{N}^i) is the path-loss exponent associated with the LOS (NLOS) link, ϕ_{L}^i (ϕ_{N}^i) is a constant, characterizing the LOS (NLOS) wireless propagation environment, and is related to various factors, e.g., the height of transceivers, antenna's beam-width, weather, etc.

In (2), for a BS located at position x_i the probability in LOS mode is $p_{n_i}^i(\|x_i\|)$, where $\sum_{n_i \in \{L,N\}} p_{n_i}^i(\|x_i\|) = 1$. For instance, ITU-R UMi model is [16], [17]

$$p_{\mathrm{L}}^i(\|x_i\|) = \min\left\{\frac{D_0^i}{\|x_i\|}, 1\right\}\left(1 - e^{-\frac{\|x_i\|}{D_1^i}}\right) + e^{-\frac{\|x_i\|}{D_1^i}}, \tag{3}$$

where, parameters D_0^i, and D_1^i characteriize the near-field (LOS), and far-field (NLOS) critical distances, respectively. Therefore, if $\|x_i\| \leq D_0^i$, BS x_i is in LOS mode. For $\|x_i\| > D_0^i$, the probability of LOS mode declines exponentially with the distance, and for $\|x_i\| > D_1^i$, it decreases quickly to 0.

A similar approach was also adopted in [22], [23], [57] to characterize $p_{\mathrm{L}}^i(\|x_i\|)$. Note that the model in (3) and similar approaches in [21], [22], [57] all have a certain level of adjustability to the communication environment (urban, dense urban, or suburban) or the clutter city (flat, scattered, hill-sided, etc.). The critical parameters of these mathematical models, such as D_0^i and D_1^i in (3), are often obtained using experimental measurements complemented by data analysis techniques, see, e.g., [57]. Therefore, some of the hidden aspects of channel modeling, such as the correlation in LOS mode—caused by large obstacles/buildings in an area which similarly affect the transmitted signals of adjacent BSs—are eventually represented in the path-loss model. (It is straightforward to confirm that the SPLM abides by (2).)

For the simulation and numerical studies we consider the path-loss attenuation function, $L_{n_i}^i(\|x_i\|) = \phi_{n_i}^i(1 + \|x_i\|)^{-\alpha_{n_i}^i}$, along with the LOS probability, (3), unless otherwise stated. Although our main focus is on the generic path-loss model, (2), with an arbitrary LOS probability, it is straightforward to extend our analysis to other models, such as multi-slope path-loss [15], and multi-ball path-loss [21].

3.2 SIR of Data Streams

In the analysis we assume the availability of perfect channel state information at the receiver (CSIR), while CSI at the transmitter (CSIT) is not available. Each BS x_i turns on S_i transmit antennas and equally divides its transmit power, P_i, among them. This transmission scheme is often referred to as *open-loop* pre-coding, see, e.g., [63], [64]. At the receiver, the system employs zero-forcing beamforming (ZFBF) [30], [63]. To decode the l_i-th stream, in ZFBF, a typical UE uses the available CSIR, $\boldsymbol{H}_{x_i}$, to mitigate the inter-stream interference. The typical UE also obtains matrix $(\boldsymbol{H}_{x_i}^{\dagger}\boldsymbol{H}_{x_i})^{-1}\boldsymbol{H}_{x_i}^{\dagger}$, where $(.)^{\dagger}$ is the conjugate transpose operator, and then multiplies the conjugate of the l_i-th column by the received signal in (1). In an interference-limited regime, i.e., ignoring noise, the post-processing SINR associated with the l_i-th stream is

$$\mathrm{SIR}_{x_i,l_i} = \frac{\frac{P_i}{S_i}L_i(\|x_i\|)H_{x_i,l_i}^{\mathrm{ZF}}}{I^{l_i}}, \tag{4}$$

where

$$I^{l_i} \triangleq \sum_{j\in\mathcal{K}}\sum_{x_j\in\Phi_j\setminus x_i}\frac{P_j}{S_j}L_j(\|x_j\|)G_{x_j,l_i}^{\mathrm{ZF}}, \tag{5}$$

is the inter-cell interference (ICI) stream l_i experienced.

As shown in [63], [64], the intended channel power gains associated with the l_i-th data stream, $H_{x_i,l_i}^{\mathrm{ZF}}$, and the ICI caused by $x_j \neq x_i$ on data stream l_i, $G_{x_j,l_i}^{\mathrm{ZF}}$, are chi-squared random variables with $2(N^r - S_i + 1)$, and $2S_j$, degrees of freedom (DoF), respectively. For each l_i, $H_{x_i,l_i}^{\mathrm{ZF}}$ and $G_{x_j,l_i}^{\mathrm{ZF}}$ are independent random variables. For for $l \neq l_i$, $H_{x_i,l_i}^{\mathrm{ZF}}$ ($G_{x_j,l_i}^{\mathrm{ZF}}$) and $H_{x_i,l}^{\mathrm{ZF}}$ ($G_{x_j,l}^{\mathrm{ZF}}$) are independent and identically distributed (i.i.d.). In (4), for a given communication link, $\mathrm{SIR}_{x_i,l_i}^{\mathrm{ZF}}$, are identical, but *not* independent across streams, see Section 5.1.

4 Coverage Probability in Multi-Stream MIMO HetNets

The *coverage probability* is defined as the probability that the SIR stays above a given SIR threshold. The coverage probability in a cellular network is often related to the complementary cumulative distribution function (CCDF) of the received SIR [9], [10], [62]. The same definition is also used in SISO and single-stream MIMO communication systems, e.g., diversity systems and space division multiple access [6], [7]. In multiple stream MIMO, we consider the coverage probability as the probability that all of a typical UE's streams are successfully decoded at the receiver. Such a notion of coverage probability is also referred to as *all-coverage probability* in isolated scenarios, e.g., [30], [31], [32], [33], [65], [66].

4.1 Cell Association

To evaluate the coverage probability, we first need to characterize the mechanism used to associate UEs with BSs. This mechanism is often referred to as *cell association* (CA). Depending on the communication scenario, application context and signaling structure, two main approaches have been proposed in the literature, including max-SIR [1], [4], [6], [32], [33], [34], [67], [68], and range expansion (a.k.a. closest-BS) [5], [7], [9].

In the closest-BS (max-CIR) CA, the BS located closest (thus providing the maximum CSI) to the user is considered as the serving BS. Our previous work [14], [34] showed that the coverage performance is substantially improved by adopting max-SIR CA. SIR-based CA is also integrated into various resource-allocation mechanisms by incorporating the physical-layer specifications, transmission policies, and scheduling and coordination across tiers, see, e.g., [36], [69], [70], [71], [72].

4.2 Coverage Probability

In a system with max-SIR, a BS is selected as the serving BS for a typical UE, if all SIRs across the streams are larger than the SIR threshold, β_i. Therefore, for a typical UE the coverage probability of ZFBF is

$$c^{\mathrm{ZF}} = \mathbb{P}\{\mathcal{A}^{\mathrm{ZF}} \neq \emptyset\}, \tag{6}$$

where

$$\mathcal{A}^{\mathrm{ZF}} = \left\{\exists i\in\mathcal{K} : \max_{x_i\in\Phi_i}\min_{l_i=1,\dots,S_i}\mathrm{SIR}_{x_i,l_i}^{\mathrm{ZF}} \geq \beta_i\right\}. \tag{7}$$

The NLOS signals are expected to be, on average, weaker than that of LOS. In some cases however, the fading fluctuation and the impact of array processing may cause the CA to select a NLOS BSs.

Evaluating c^{ZF}, for LOS/NLOS, is challenging due to the following issues. First, for each data stream, the fading fluctuation in the intended signal is chi-squared, which often results in a less tractable analysis than that of Rayleigh fading. Second, the unconventional LOS/NLOS path-loss model exacerbates the complexity of analysis. Third, the ICI correlation across data streams in a communication link further interrelates the stream and link coverage probabilities. The cross-stream ICI correlation is created by the existence of the same interferers across data streams, see Section 5.1.

Therefore, conditioned on $G_{x_j,l_i}^{\mathrm{ZF}}$, $\forall l_i$, the interference originated from BS x_j, depends on $L_j(\|x_j\|)$, which is a random variable (r.v.) independent of data stream l_i. In [30], [33], we have already developed analytical tools that enable us to deal with the first and the third issues above in cases with SPLM. In what follows, we use this to obtain the coverage probability in cases with the LOS/NLOS path-loss model, addressing the above three issues.

Proposition 1: The coverage probability of a multi-stream MIMO-ZFBF cellular network with LOS/NLOS path-loss, (2), is

$$c^{\mathrm{ZF}} = \sum_{i\in\mathcal{K}}2\pi\lambda_i\sum_{m_1=0}^{N^r-S_i}\dots\sum_{m_{S_i}=0}^{N^r-S_i}\frac{(-1)^{m_1+\dots+m_{S_i}}}{m_1!\dots m_{S_i}!}\int_0^{\infty}r_i\mathrm{d}r_i$$
$$\left.\frac{\partial^{m_1}\dots\partial^{m_{S_i}}\left(\sum_{n\in\{\mathrm{L,N}\}}p_n^i(r_i)\overline{\Psi}_n^i(r_i)\right)}{\partial {t_{l_1}}^{m_1}\dots\partial {t_{l_{S_i}}}^{m_{l_{S_i}}}}\right|_{t_{l_i}=1,\forall l_i},$$

where for each $n\in\{\mathrm{L,N}\}$,

$$\overline{\Psi}_n^i(r_i) = \exp\left(-2\pi\sum_{j=1}^{K}\lambda_j\int_0^{\infty}y_j\big(1-\Psi_n^i(r_i,y_j)\big)dy_j\right),$$

$$\Psi^i_n(r_i, y_j) = \sum_{n' \in \{\mathrm{L,N}\}} p^j_{n'}(y_j) \prod_{l_i=1}^{S_i} (1 + \frac{\beta_i S_i P_j L^j_{n'}(y_j)}{S_j P_i L^i_n(r_i)} t_{l_i})^{-S_i}$$

Proof: See Appendix A. ■

The coverage probability in Proposition 1 is a function of tiers' BS densities, their SIR thresholds, transmission powers, and multiplexing gains. The impact of of LOS, and NLOS path-loss for the intended link are captured by functions $\overline{\Psi}^i_{\mathrm{N}}(r_i)$, and $\overline{\Psi}^i_{\mathrm{N}}(r_i)$, respectively. Furthermore, $\overline{\Psi}^i_{\mathrm{N}}(r_i)$ and $\overline{\Psi}^i_{\mathrm{N}}(r_i)$, are functions of the LOS/NLOS modes of the interfering links, respectively, through $\Psi^i_{\mathrm{L}}(r_i, y_j)$, and $\Psi^i_{\mathrm{N}}(r_i, y_j)$.

As a key performance parameter, the coverage probability is often required to be calculated many times in various resource-allocation schemes to find the best combination of the network operational parameters. Calculating the coverage probability in Proposition 1 is, however, challenging due to the requirement of extensive numerical calculations. Thus, we propose several approximations of the coverage probability with acceptable accuracy and reasonable computational complexity.

5 Coverage Probability Approximation

The link-level coverage probability, as defined in Section 3, is directly related to the SIR of every single stream in that link. The SIR values for streams are, however, strongly correlated due to cross-stream ICI correlation. Therefore, to evaluate the coverage probability, we first need to quantify the cross-stream ICI correlation.

5.1 Cross-Stream ICI Correlation

We use Pearson correlation coefficients to characterize the ICI correlation between streams $l_i \neq l'_i$:

$$\rho_{l_i,l'_i} = \frac{\mathbb{E}[I^{l_i} I^{l'_i}] - \mathbb{E}[I^{l_i}]\mathbb{E}[I^{l'_i}]}{\sqrt{\mathrm{Var}(I^{l_i})\mathrm{Var}(I^{l'_i})}}, \tag{8}$$

where $\mathrm{Var}(x)$ is the variance of random variable x. We further note that the ICI is an identical shot-noise process across streams, so ρ_{l_i,l'_i} is[1]

$$\rho_{l_i,l'_i} = \frac{\mathbb{E}[I^{l_i} I^{l'_i}] - (\mathbb{E}[I^{l_i}])^2}{\mathrm{Var}(I^{l_i})}. \tag{9}$$

Proposition 2: For a MIMO-ZFBF multiplexing system with the generic LOS/NLOS pathloss,

$$\rho_{l_i,l'_i} = \frac{\sum\limits_{j \in \mathcal{K}} P_j^2 \lambda_j \sum\limits_{n_j \in \{\mathrm{L,N}\}} \int\limits_0^\infty r_j p^j_{n_j}(r_j)(L^j_{n_j}(r_j))^2 \mathrm{d}r_j}{\sum\limits_{j \in \mathcal{K}} P_j^2 \frac{S_j(S_j+1)-1}{S_j^2} \lambda_j \sum\limits_{n_j \in \{\mathrm{L,N}\}} \int\limits_0^\infty r_j p^j_{n_j}(r_j)(L^j_{n_j}(r_j))^2 \mathrm{d}r_j}. \tag{10}$$

Proof: See Appendix B. ■

1. Interference correlation is studied in [50], [62], [73], focusing on quantifying the impact of interference correlation on the time and receive-array diversities. Here we are interested in quantifying the impact of multiplexing gains and NLOS/NLOS path-loss model on the interference correlation. We also use this analysis to corroborate the validity of the full-correlation (FC) assumption for approximating the coverage probability.

For a single tier network, $K = 1$, Proposition 2 results in the following corollary.

Corollary 1: For a single tier MIMO-ZFBF,

$$\rho_{l_1,l'_1} = \frac{S_1^2}{S_1(S_1+1)-1}, \tag{11}$$

which only depends on the multiplexing gain.

Proposition 3: In a MIMO-ZFBF multiplexing system,

$$0.5 \leq \frac{1}{1 + \max_i \frac{S_i - 1}{S_i^2}} \leq \rho_{l_i,l'_i} \leq \frac{1}{1 + \min_i \frac{S_i - 1}{S_i^2}} \leq 1. \tag{12}$$

Proof: See Appendix C. ■

Proposition 3 shows that in the MIMO multiplexing system, ρ_{l_i,l'_i} is larger than 0.5, so ICI is highly correlated across data streams. In Fig. (2-a), we illustrate ρ_{l_1,l'_1} vs. S_1 for a simulated system. ICIs across data streams are shown to be significantly correlated. Fig. (2-a) also confirms the validity of the bound in Proposition 3.

Also, Fig. (2-a) shows that for $S_1 > 2$ ($S_1 < 2$), ρ_{l_1,l'_1} is an increasing (decreasing) function of S_1, and its maximum (minimum) occurs at $S_1 = 2$. Setting the derivative of (**??**) to zero, one can analytically obtain $S_1 = 2$:

$$\frac{\partial \rho_{l_1,l'_1}}{\partial S_1} = \frac{\sum\limits_{j \in \mathcal{K}} \lambda_j A_j}{\left(\sum\limits_{j \in \mathcal{K}} \lambda_j A_j \frac{S_j(S_j+1)-1}{S_j^2} \right)^2} \frac{S_1(S_1-2)}{S_1^4} = 0. \tag{13}$$

In Fig. (2-b), we present ρ_{l_1,l'_1} vs. α^2_{L}. ρ_{l_1,l'_1} in (2-b) is shown to vary within the bounds given in Proposition 3. Fig. (2-b) shows ρ_{l_1,l'_1} to be also highly correlated across streams, and an increasing function of α^2_{L}. This is also stated in the following corollary.

Corollary 2: Increasing α^2_{L} results in a higher ρ_{l_1,l'_1} for any combination of multiplexing gains for which

$$\sum_{j \in \mathcal{K}} \lambda_j A_j \frac{S_j(S_j+1)-1}{S_j^2} > \frac{S_2(S_2+1)-1}{S_2^2} \sum_{j \in \mathcal{K}} \lambda_j A_j. \tag{14}$$

Proof: See Appendix D. ■

The system considered for the simulation in Fig. (2-b) is a two-tier system, $K = 2$. For this system (14) is reduced to:

$$\frac{S_1(S_1+1)-1}{S_1^2} > \frac{S_2(S_2+1)-1}{S_2^2},$$

which holds if $S_1 > S_2 > 2$.[2] That is, for any $S_1 > S_2 > 2$, $\frac{\partial \rho_{l_1,l'_1}}{\partial \alpha^2_{\mathrm{L}}} > 0$.

5.2 Full Correlation Assumption

Our analysis in Section 5.1 indicates that the ICI is highly correlated across the streams, justifying the construction of 'full-correlation' (FC) approximation, where the ICI across all streams in a given communication link is considered fully correlated, i.e., $\rho_{l_i,l'_i} = 1$. Such an assumption has also been used for analyzing other aspects of MIMO systems in [32], [33], [43].

2. This is because $g(x) = \frac{x(x+1)-1}{x^2}$ is an increasing function of x for for $x > 2$.

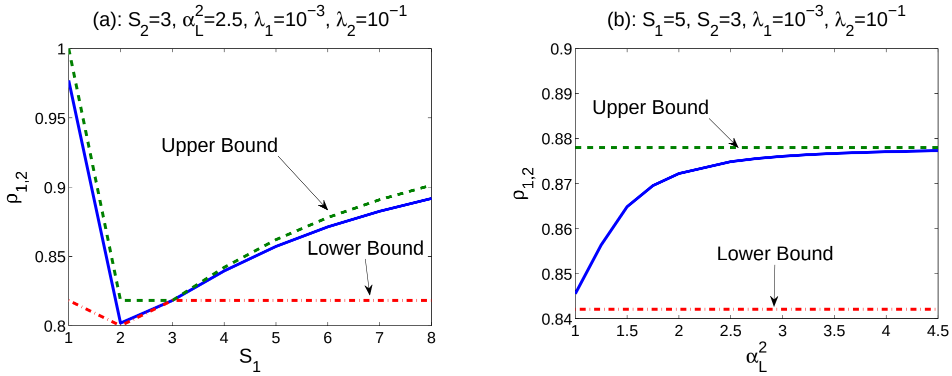

Fig. 2. Cross-stream ICI correlation coefficient vs. S_1, α_L^2, the simulation results and bounds, in a system with $K = 2$, $\alpha_{\mathrm{N}}^1 = 3.75$, $\alpha_{\mathrm{N}}^2 = 4.75$, $P_1 = 25$ W, $P_2 = 1$ W, $N_1^t = 16$, $N_2^t = 8$, $N^r = 8$, $D_0^1 = 36$, $D_0^2 = 9$, $D_1^1 = 48$, $D_1^2 = 18$ meter, and $\phi_{\mathrm{L}}^i = \phi_{\mathrm{N}}^i = 1$.

Assuming FC, ICI for the typical UE associated with BS x_i is

$$I^{\mathrm{FC}} = \sum_{j\in\mathcal{K}} \sum_{x_j\in\Phi_j\setminus x_i} \frac{P_j}{S_j} L_j(\|x_j\|) G_{x_j}^{\mathrm{ZF}}, \tag{15}$$

where for $l_i = 1, 2, \ldots, S_i$ we simply replace the interfering channel power gain, $G_{x_j,l_i}^{\mathrm{ZF}}$, with $G_{x_j}^{\mathrm{ZF}}$ (both chi-squared r.v.s with $2S_j$ DoFs). For data stream l_i, the post-processing SIR is then approximated as

$$\mathrm{SIR}_{x_i,l_i}^{\mathrm{ZF-FC}} = \frac{\frac{P_i}{S_i} L_i(\|x_i\|) H_{x_i,l_i}^{\mathrm{ZF}}}{I^{\mathrm{FC}}}. \tag{16}$$

Therefore, for the max-SIR CA under the FC assumption, the max-SIR CA rule 7 is rewritten as

$$\mathcal{A}^{\mathrm{ZF-FC}} = \left\{ \exists i \in \mathcal{K} : \max_{x_i\in\Phi_i} \frac{\frac{P_i}{S_i} L_i(\|x_i\|) H_{x_i,\min}^{\mathrm{ZF}}}{I^{\mathrm{FC}}} \geq \beta_i \right\}, \tag{17}$$

$H_{x_i,\min}^{\mathrm{ZF}} \triangleq \min_{l_i=1,\ldots,S_i} H_{x_i,l_i}^{\mathrm{ZF}}$. This implies that the probability of coverage for the typical UE is $c^{\mathrm{ZF-FC}} = \Pr\left\{\mathcal{A}^{\mathrm{ZF-FC}} \neq \emptyset\right\}$. Similarly to Appendix A, we then use Lemma 1 in [4] to derive the coverage probability as

$$\begin{aligned}
c^{\mathrm{ZF-FC}} &= \mathbb{P}\left\{ \max_{\bigcup_{i\in\mathcal{K}} x_i\in\Phi_i} \frac{\frac{P_i}{S_i} L_i(\|x_i\|) H_{x_i,\min}^{\mathrm{ZF}}}{I^{\mathrm{FC}}} \geq \beta_i \right\} \\
&= \sum_{i\in\mathcal{K}} \mathbb{E} \sum_{x_i\in\Phi_i} 1\left(\frac{\frac{P_i}{S_i} L_i(\|x_i\|) H_{x_i,\min}^{\mathrm{ZF}}}{I^{\mathrm{FC}}} \geq \beta_i \right) \\
&= \sum_{i\in\mathcal{K}} 2\pi\lambda_i \int_0^\infty r_i \mathbb{P}\left\{ \frac{\frac{P_i}{S_i} L_i(r_i) H_{x_i,\min}^{\mathrm{ZF}}}{I^{\mathrm{FC}}} \geq \beta_i \right\} \mathrm{d}r_i \\
&= \sum_{i\in\mathcal{K}} 2\pi\lambda_i \int_0^\infty r_i \mathbb{E}_{L_i(r_i),\Phi,\{L_j(\|x_j\|)\}_{\forall x_j,j}} \mathbb{P}\Big\{ H_{x_i,\min}^{\mathrm{ZF}} \geq \\
&\qquad \frac{\beta_i I^{\mathrm{FC}}}{\frac{P_i}{S_i} L_i(r_i)} \big| \Phi, L_i(r_i), \{L_j(\|x_j\|)\}_{\forall x_j,j} \Big\} \mathrm{d}r_i.
\end{aligned} \tag{18}$$

Evaluating the coverage probability based on (18) is shown to be a complicated task. To address this difficulty, we propose two approximations for (18) which enable the numerical evaluation of the coverage probability as a function of the main system parameters.

5.2.1 *Alzer Approximation*

Alzer's inequality [56], [57] (see Appendix-C Lemma 1) has been used to evaluate the coverage probability under Nakagami-type fading and multi-user MIMO systems using stochastic geometry. Here, for the first time we extend Alzer's inequality to approximate the coverage probability of a multi-stream multi-tier MIMO-ZFBF system. We refer to this method as A-A, where Alzer's lemma is utilized to approximate the effective power gain of the attending channel for each data stream as an exponential random variable. This is presented in the following Proposition.

Proposition 4: In a multi-stream MIMO-ZFBF cellular system with LOS/NLOS pathloss model, and $S_i' = ((N^r - S_i + 1)!)^{-\frac{1}{(N^r - S_i + 1)}}$, the coverage probability is approximated as

$$\begin{aligned}
c^{\mathrm{A-A}} &= \sum_{i\in\mathcal{K}} 2\pi\lambda_i \Bigg(1 + \sum_{l_i'=1}^{S_i} \sum_{l_i''=0}^{(N^r-S_i+1)l_i'} (-1)^{l_i'+l_i''} \times \\
&\binom{(N^r - S_i + 1)l_i'}{l_i''} \binom{S_i}{l_i'} \sum_{n_i\in\mathrm{L,N}} \int_0^\infty r_i p_{n_i}^i(r_i) \widehat{\Psi}_{n_i}^i(r_i) \mathrm{d}r_i \Bigg),
\end{aligned} \tag{19}$$

where $\widehat{\Psi}_{n_i}^i(r_i) = \exp\left(-2\pi \sum_j \lambda_j \int_0^\infty y_j (1 - \widehat{\Psi}_{n_i}^i(r_i, y_j)) dy_j \right)$,

$$\widehat{\Psi}_{n_i}^i(r_i, y_j) = \sum_{n_j\in\{\mathrm{L,N}\}} \frac{p_{n_j}^j(y_j)}{\left(1 + S_i' l_i'' \frac{\beta_i S_i P_j L_{n_j}^j(y_j)}{S_j P_i L_{n_i}^i(r_i)}\right)^{S_j}}.$$

Proof: See Appendix E. ■

The numerical complexity of obtaining $c^{\mathrm{A-A}}$ in Proposition 4 is significantly lower than that of Proposition 1 as there are no concatenated higher-order differentiations. The impact of LOS/NLOS model parameters on the intended and interfering links can be seen in $\widehat{\Psi}_{\mathrm{L}}^i(r_i)$/ $\widehat{\Psi}_{\mathrm{N}}^i(r_i)$, and $\widehat{\Psi}_{\mathrm{L}}^i(r_i, y_j)/\widehat{\Psi}_{\mathrm{N}}^i(r_i, y_j)$.

5.2.2 *Gamma Approximation*

The coverage probability, $c^{\mathrm{ZF-FC}}$, is

$$c^{\mathrm{ZF-FC}} = \sum_{i\in\mathcal{K}} 2\pi\lambda_i \sum_{n_i\in\mathrm{L,N}} \int_0^\infty r_i p_{n_i}^i(r_i) \times$$

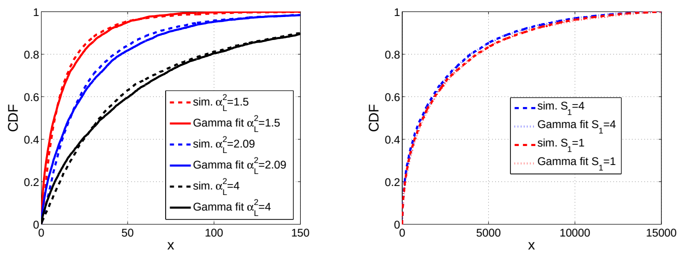

Fig. 3. CDF of $\frac{1}{I^{\rm FC}}$, (a): $\lambda_1 = 10^{-4}$, $\lambda_2 = 10^{-3}$, $S_1 = 2$, $S_2 = 2$, $\alpha^1_{\rm L} = 2.09$, $\alpha^1_{\rm N} = 3.75$, $\alpha^2_{\rm N} = 4.75$, $P_1 = 50$W, $P_2 = 10$W, $N^t_1 = 16$, $N^t_2 = 8$, $N^r = 8$, and $\phi^i_{\rm L} = \phi^i_{\rm N} = 1$; (b) $\lambda_1 = 10^{-4}$, $\lambda_2 = 10^{-3}$, $S_2 = 2$, $\alpha^1_{\rm L} = 2.09$, $\alpha^1_{\rm N} = 3.75$, $\alpha^2_{\rm L} = 1.5$, $\alpha^2_{\rm N} = 4.75$, $P_1 = 50$W, $P_2 = 10$W, $N^t_1 = 16$, $N^t_2 = 8$, $N^r = 8$, and $\phi^i_{\rm L} = \phi^i_{\rm N} = 1$.

$$\mathbb{E}_{I^{\rm FC}}\mathbb{P}\left\{\frac{H^{\rm ZF}_{x_i,\min}}{I^{\rm FC}} \geq \frac{\beta_i}{\frac{P_i}{S_i}L^i_{n_i}(r_i)}\Big|\Phi, I^{\rm FC}\right\}{\rm d}r_i. \tag{20}$$

Instead of the intended fading gain, one may approximate the statistical characteristics of $I^{\rm FC}$. Note, however, that in the max-SIR CA, in some cases the interferers are even closer to the typical UE than the serving BS. This can happen, for instance, in LOS mode with a very small LOS path-loss exponent. For LOS path-loss functions, where $L^i_{\rm L}(x) \propto x^{-\alpha^i_{\rm L}}$, the mean and variance of $I^{\rm FC}$ could be very high. Instead, we model $\frac{1}{I^{\rm FC}}$.

The CDF of $\frac{1}{I^{\rm FC}}$ is plotted in Fig. (3) for the simulated system with the parameters given in the caption. Fig. (3-a) shows that for different values of the LOS path-loss exponent, the CDF closely follows the Gamma distribution. Fig. (3-b) further shows that the approximation based on Gamma distribution remains valid for various multiplexing gains. This has also been confirmed for a variety of other system parameters which are not reported here due to space limitation.

Based on the above, we approximate the CDF of $\frac{1}{I^{\rm FC}}$ by a Gamma distribution, $\frac{1}{I^{\rm FC}} \propto {\rm Gamma}(a, b)$, where, adopting a moment-matching technique, parameters a and b are obtained as

$$a = \frac{(\mathbb{E}\frac{1}{I^{\rm FC}})^2}{(\mathbb{E}\frac{1}{(I^{\rm FC})^2} - (\mathbb{E}\frac{1}{I^{\rm FC}})^2)}, \tag{21}$$

$$b = \frac{\mathbb{E}\frac{1}{I^{\rm FC}}}{(\mathbb{E}\frac{1}{(I^{\rm FC})^2} - (\mathbb{E}\frac{1}{I^{\rm FC}})^2)}. \tag{22}$$

For a ${\rm Gamma}(a, b)$ random variable with pdf $f_X(x) = \frac{b^a}{\Gamma(a)}x^{a-1}e^{-bx}$, $\overline{X} = \frac{a}{b}$ and ${\rm Var}(X) = \frac{a}{b^2}$. To obtain a and b, we need to calculate $\mathbb{E}\frac{1}{I^{\rm FC}}$ and $\mathbb{E}\frac{1}{(I^{\rm FC})^2}$. The former is given by

$$\mathbb{E}\frac{1}{I^{\rm FC}} = \mathbb{E}\int_0^\infty e^{-vI^{\rm FC}}dv = \int_0^\infty \widetilde{\Psi}(v)dv, \tag{23}$$

where $\widetilde{\Psi}(v)$ is the Laplace transform of $I^{\rm FC}$:

$$\widetilde{\Psi}(v) = \mathbb{E}e^{-v\sum\limits_{j\in\mathcal{K}}\sum\limits_{x_j\in\Phi_j\backslash x_i}\frac{P_j}{S_j}L_j(\|x_j\|)G^{\rm ZF}_{x_j}}$$

$$= \prod_{j\in\mathcal{K}}\mathbb{E}_{\Phi_j}\prod_{x_j\in\Phi_j\backslash x_i}\mathbb{E}_{G^{\rm ZF}_{x_j}, L_j(\|x_j\|)}e^{-v\frac{P_j}{S_j}L_j(\|x_j\|)G^{\rm ZF}_{x_j}}$$

$$= \prod_{j\in\mathcal{K}}\mathbb{E}_{\Phi_j}\prod_{x_j\in\Phi_j\backslash x_i}\sum_{n_j\in\{{\rm L},{\rm N}\}}\frac{p^j_{n_j}(\|x_j\|)}{\left(1+v\frac{P_j}{S_j}L^j_{n_j}(\|x_j\|)\right)^{S_j}}$$

$$= \exp(-2\pi\sum_j\lambda_j\int_0^\infty y_j(1-\widetilde{\Psi}_{\rm ZF}(v, y_j))dy_j), \tag{24}$$

where

$$\widetilde{\Psi}_{\rm ZF}(v, y_j) = \sum_{n_j\in{\rm L},{\rm N}}\frac{p^j_{n_j}(y_j)}{\left(1+\frac{P_j}{S_j}L^j_{n_j}(y_j)\right)^{S_j}}. \tag{25}$$

Note that in $\widetilde{\Psi}_{\rm ZF}(v, y_j, S_j)$ the first (second) term is associated with the LOS (NLOS) mode of the BS located at y_j. Similarly, the second moment of $\frac{1}{I^{\rm FC}}$ is:

$$\mathbb{E}\frac{1}{(I^{\rm FC})^2} = \mathbb{E}\int_0^\infty\int_0^\infty e^{-(v_1+v_2)I^{\rm FC}}dv_1dv_2 =$$

$$\int_0^\infty\int_0^\infty \widetilde{\Psi}(v_1+v_2)dv_1dv_2 = \int_0^\infty v\widetilde{\Psi}(v)dv. \tag{26}$$

Using the above, in the following we approximate the coverage probability using Gamma distribution, which will henceforth be called G-A.

Proposition 5: We define

$$\overline{\sum}_{i,\boldsymbol{k}} \triangleq \sum_{k_0+k_2+\ldots+k_{N^r-S_i}=S_i-1}\binom{S_i-1}{k_0, k_2, \ldots, k_{N^r-S_i}},$$

and $\tilde{S}_i(\boldsymbol{k}) \triangleq N^r - S_i + 1 + \sum\limits_{l=0}^{N^r-S_i} lk_l$. An approximation, namely G-A, of the coverage probability in a multi-stream MIMO-ZFBF cellular network with an LOS/NLOS attenuation, (2), is

$$c^{\rm G-A} = \sum_{i\in\mathcal{K}}\frac{2\pi\lambda_i S_i}{(N^r-S_i)!\Gamma(a)}\sum_{n_i\in\{{\rm L},{\rm N}\}}\overline{\sum}_{i,\boldsymbol{k}}$$

$$\times\int_0^\infty\int_0^\infty r_i p^i_{n_i}(r_i)\frac{h^{\tilde{S}_i(\boldsymbol{k})-1}e^{-S_ih}}{\prod\limits_{l=0}^{N^r-S_i}(l!)^{k_l}}\gamma\left(a, b\frac{\beta_i}{\frac{P_i}{S_i}L^i_{n_i}(r_i)h}\right){\rm d}r_i{\rm d}h \tag{27}$$

where $\gamma(a, bx)$ is the CDF of random variable ${\rm Gamma}(a, b)$.

Proof: See Appendix F. ■

Compared to Proposition 1, in Proposition 4 the numerical complexity of obtaining an approximation of the coverage probability is substantially reduced. Nevertheless, the numerical complexity of obtaining $c^{\rm G-A}$ is higher than that of $c^{\rm A-A}$, because in G-A, a and b should also be obtained as in (21) and (22), respectively. G-A further requires the calculation of double integration which is not required in A-A, see (46).

In G-A, a and b are tier-independent—once they are obtained for a given setting (density of BSs, transmission powers, multiplexing gains, and LOS/NLOS parameters), they are valid regardless of the tier that the typical UE is associated with. This substantially reduces the computational cost of evaluating (52).

The simulation results in Section 7 reveal that the extra complexity of G-A brings a higher accuracy and robustness over a wide range of system parameters. Compared to A-A, G-A also captures the actual behavior of the coverage probability against densification more precisely. Further, as shown in Section 7, G-A enables accurate evaluation of BSs' density for which the maximum coverage performance is achieved.

6 Special Cases

We use the results derived for open-loop ZFBF MIMO multiplexing system to evaluate the coverage performance in MIMO diversity only, ZFBF with nonhomogeneous and homogenous SPLM, and systems with available CSIT (full CSIT and quantized CSIT). The main objective is to demonstrate how one can derive the coverage probability of various MIMO system settings using the analytical framework developed in this paper. The analytical results here are supported further by the simulations and numerical results in Section 7.

6.1 Diversity Only Systems

In this type of systems, $S_i = 1, \forall i$, i.e., single-stream MIMO or single-input multiple-output (SIMO) systems.

A-A Method: Proposition 4 is reduced to

$$c^{\mathrm{SIMO-A-A}} = \sum_{i\in\mathcal{K}} 2\pi\lambda_i \Bigg(1 + S_i \sum_{l_i''=0}^{N^r} \binom{N^r}{l_i''} (-1)^{l_i''+1} \sum_{n_i\in\{\mathrm{L,N}\}} \int_0^\infty r_i p_{n_i}^i(r_i) \widehat{\Psi}_{n_i}^i(r_i) \mathrm{d}r_i\Bigg), \tag{28}$$

where $\widehat{\Psi}_{n_i}^i(r_i)$ is defined as

$$\widehat{\Psi}_{n_i}^i(r_i, y_j) = \sum_{n_j\in\{\mathrm{L,N}\}} \frac{p_{n_j}^j(y_j)}{\left(1 + (N^r!)^{-\frac{1}{N^r}} l_i'' \frac{\beta_i P_j L_{n_j}^j(y_j)}{P_i L_{n_i}^i(r_i)}\right)^{S_j}}.$$

G-A Method: Using Proposition 5, G-A approximation implies that

$$c^{\mathrm{SIMO-G-A}} = \sum_{i\in\mathcal{K}} \frac{2\pi\lambda_i}{(N^r-1)!\Gamma(a)} \sum_{n_i\in\{\mathrm{L,N}\}} \times \int_0^\infty \int_0^\infty r_i p_{n_i}^i(r_i) h^{N^r-1} e^{-h} \gamma\left(a, b\frac{\beta_i}{P_i L_{n_i}^i(r_i) h}\right) \mathrm{d}r_i \mathrm{d}h, \tag{29}$$

where

$$a = \frac{(\mathbb{E}\frac{1}{I^{\mathrm{FC}}})^2}{(\mathbb{E}\frac{1}{(I^{\mathrm{FC}})^2} - (\mathbb{E}\frac{1}{I^{\mathrm{FC}}})^2)}, \tag{30}$$

$$b = \frac{\mathbb{E}\frac{1}{I^{\mathrm{FC}}}}{(\mathbb{E}\frac{1}{(I^{\mathrm{FC}})^2} - (\mathbb{E}\frac{1}{I^{\mathrm{FC}}})^2)}, \tag{31}$$

and

$$\mathbb{E}\frac{1}{I^{\mathrm{FC}}} = \int_0^\infty \exp(-2\pi \sum_j \lambda_j \int_0^\infty y_j(1 - \widetilde{\Psi}_{\mathrm{D}}(v, y_j)) dy_j) dv, \tag{32}$$

$$\mathbb{E}\frac{1}{(I^{\mathrm{FC}})^2} = \int_0^\infty v \exp(-2\pi \sum_j \lambda_j \int_0^\infty y_j(1 - \widetilde{\Psi}_{\mathrm{D}}(v, y_j)) dy_j) dv, \tag{33}$$

where $\widetilde{\Psi}_{\mathrm{D}}(v, y_j)$ is defined similarly to (25), where $S_j = 1$.

6.2 ZFBF Multiplexing with Non-homogeneous SPLM

In non-homogeneous SPLM, $\alpha_L^i = \alpha_N^i = \alpha_i$ and $\phi_L^i = \phi_N^i$, $\forall i$.

A-A Method: It is straightforward to show that the approximation of the coverage probability based on A-A is

$$c^{\mathrm{A-A}} = \sum_{i\in\mathcal{K}} 2\pi\lambda_i \Bigg(1 + \sum_{l_i'=1}^{S_i} \sum_{l_i''=0}^{(N^r-S_i+1)l_i'} \binom{(N^r-S_i+1)l_i'}{l_i''} (-1)^{l_i'+l_i''} \binom{S_i}{l_i'} \int_0^\infty r_i e^{-2\pi\sum_j \frac{\lambda_j W(\alpha_j) r_i^{2\frac{\alpha_i}{\alpha_j}}}{\alpha_j (S_i' l_i'' \frac{\beta_i S_i P_j}{P_i})^{2+\frac{2}{\alpha_j}}}} \mathrm{d}r_i, \tag{34}$$

where $W(\alpha_j) = \int_0^\infty w^{-1-\frac{2}{\alpha_j}}(1 - e^{-w})\mathrm{d}w$.

G-A Method: Using Proposition 5,

$$c^{\mathrm{G-A}} = \sum_{i\in\mathcal{K}} \frac{2\pi\lambda_i S_i}{(N^r - S_i)!\Gamma(a)} \overline{\sum}_{i,\boldsymbol{k}} \times \int_0^\infty \int_0^\infty r_i \frac{h^{\tilde{S}_i(\boldsymbol{k})-1} e^{-S_i h}}{\prod_{l=0}^{N^r-S_i} (l!)^{k_l}} \gamma\left(a, b\frac{\beta_i r_i^{\alpha_i}}{\frac{P_i}{S_i} h}\right) \mathrm{d}r_i \mathrm{d}h, \tag{35}$$

where parameters a and b are defined, respectively, in (30) and (31). To derive these parameters, we should replace $\widetilde{\Psi}_{\mathrm{ZF}}(v, y_j)$ in (25) with $\widetilde{\Psi}_{\mathrm{ZF-Nonhomogeneous}}(v, y_j) = \frac{1}{\left(1+\frac{P_j}{S_j} y_j^{-\alpha_j}\right)^{S_j}}$, along with (32) and (33).

6.3 ZFBF Multiplexing with Homogeneous Standard Path-Loss Model

In Homogeneous SPLM, $\alpha_i = \alpha \; \forall i$.

A-A Method: One may start with (34) and apply a straightforward integration, to show that the coverage probability is approximated as

$$c^{\mathrm{A-A}} = \frac{\alpha}{W(\alpha) \sum_j \lambda_j P_j^{\breve{\alpha}}} \sum_{i\in\mathcal{K}} \frac{\lambda_i (\frac{P_i}{\beta_i S_i})^{2+\breve{\alpha}}}{(S_i')^{2+\breve{\alpha}}} \Bigg(1 + \sum_{l_i'=1}^{S_i} \sum_{l_i''=0}^{(N^r-S_i+1)l_i'} (-1)^{l_i'+l_i''} \binom{S_i}{l_i'} \binom{(N^r - S_i + 1)l_i'}{l_i''} l_i''^{2+\breve{\alpha}}\Bigg).$$

This expression is similar to the upper-bound provided in Proposition 1 in [30]:

$$c^{\mathrm{ZF}} \le \frac{\pi}{\tilde{C}(\alpha)} \sum_{i\in\mathcal{K}} \frac{\lambda_i \left(\frac{P_i}{S_i^2 \beta_i}\right)^{\breve{\alpha}} \left(\sum_{r_i=0}^{N^r-S_i} \frac{\Gamma(\frac{\breve{\alpha}}{S_i}+r_i)}{\Gamma(\frac{\breve{\alpha}}{S_i})\Gamma(1+r_i)}\right)^{S_i}}{\sum_{j\in\mathcal{K}} \lambda_j \left(\frac{P_j}{S_j}\right)^{\breve{\alpha}} \left(\frac{\Gamma(\frac{\breve{\alpha}}{S_i}+S_j)}{\Gamma(S_j)}\right)^{S_i}}, \tag{36}$$

where $\tilde{C}(\alpha) = \pi\Gamma(1 - \breve{\alpha})$. It is interesting to observe some resemblance between (36) and $c^{\mathrm{A-A}}$.

G-A Method: Proposition 5 yields:

$$c^{\mathrm{G-A}} = \sum_{i\in\mathcal{K}} \frac{2\pi\lambda_i S_i}{(N^r - S_i)!\Gamma(a)} \overline{\sum}_{i,\boldsymbol{k}}$$

$$\times \int_0^\infty \int_0^\infty r_i \frac{h^{\tilde{S}_i(\boldsymbol{k})-1} e^{-S_i h}}{\prod_{l=0}^{N^r - S_i} (l!)^{k_l}} \gamma\left(a, b\frac{\beta_i r_i^\alpha}{\frac{P_i}{S_i} h}\right) \mathrm{d}r_i \mathrm{d}h, \tag{37}$$

where parameters a and b are defined in (30) and (31), respectively. To derive these parameters, we set $\widetilde{\Psi}_{\mathrm{ZF}}(v, y_j)$ in (25) with $\widetilde{\Psi}_{\mathrm{ZF-Homogeneous}}(v, y_j) = \frac{1}{\left(1 + \frac{P_j}{S_j} y_j^{-\alpha}\right)^{S_j}}$, along with (32) and (33).

6.4 Known CSIT

In the above derivations, we simply assume that the CSIT is not known to the BSs. However, there are practical scenarios that CSIT is available to BSs. So, our analysis is shown to cover such cases as well.

6.4.1 Single-Input Single-Output (SISO) Systems

For a SISO system, $S_i = N_i^t = N^r = 1$ and Proposition 1 yields:

$$c^{\mathrm{SISO}} = \sum_{i\in\mathcal{K}} 2\pi\lambda_i \sum_{n\in\{\mathrm{L,N}\}} \int_0^\infty r_i p_n^i(r_i) \exp(-2\pi \sum_{j=1}^K \lambda_j$$

$$\int_0^\infty y_j \big(1 - \Psi_n(r_i, y_j)\big) dy_j) \mathrm{d}r_i,$$

where

$$\Psi_n(r_i, y_j) = \sum_{n'\in\{\mathrm{L,N}\}} p_{n'}^j(y_j)(1 + \frac{\beta_i P_j L_{n'}^j(y_j)}{P_i L_n^i(r_i)})^{-1}.$$

Note that for this scenario, both A-A and Proposition 1 yield the same coverage performance.

G-A Method: Using Proposition 5,

$$c^{\mathrm{SISO-G-A}} = \sum_{i\in\mathcal{K}} \frac{2\pi\lambda_i}{\Gamma(a)} \sum_{n_i\in\{\mathrm{L,N}\}}$$

$$\times \int_0^\infty \int_0^\infty r_i p_{n_i}^i(r_i) e^{-h} \gamma\left(a, b\frac{\beta_i}{P_i L_{n_i}^i(r_i) h}\right) \mathrm{d}r_i \mathrm{d}h, \tag{38}$$

where a, and b are defined in (30), and (31), respectively. To derive these parameters, one should replace $\widetilde{\Psi}_{\mathrm{ZF}}(v, y_j)$ in (25) with $\widetilde{\Psi}_{\mathrm{SISO}}(v, y_j) = \sum_{n_j\in\mathrm{L,N}} \frac{p_{n_j}^j(y_j)}{\left(1 + P_j L_{n_j}^j(y_j)\right)}$, along with (32) and (33).

6.4.2 Multiple-Input Single-Output (MISO) Systems

In a MISO system, $N^r = 1$, and $S_i = 1$, $\forall i$. We assume that available CSIT at the BSs is utilized for eigen-beamforming, i.e., maximum ratio transmission (MRT) [74]. In this system, the SIR at the typical UE served by BS x_i is

$$\mathrm{SIR}_{x_i}^{\mathrm{MRT}} = \frac{P_i L_i(\|x_i\|) H_{x_i}^{\mathrm{MRT}}}{\sum_{j\in\mathcal{K}} \sum_{x_j\in\Phi_j/x_i} P_j L_j(\|x_j\|) G_{x_j}^{\mathrm{MRT}}}, \tag{39}$$

where $H_{x_i}^{\mathrm{MRT}}$ and $G_{x_j}^{\mathrm{MRT}}$ are chi-squared with $2N_i^t$ DoFs, and exponential random variables, respectively.

A-A Method: Using Proposition 4,

$$c^{\mathrm{MRT-A-A}} = \sum_{i\in\mathcal{K}} 2\pi\lambda_i \Bigg(1 + \sum_{l_i''=0}^{N^r} (-1)^{l_i''+1}$$

$$\binom{N^r}{l_i''} \sum_{n_i\in\mathrm{L,N}} \int_0^\infty r_i p_{n_i}^i(r_i) \widehat{\Psi}_{n_i}^i(r_i) \mathrm{d}r_i\Bigg), \tag{40}$$

where $\widehat{\Psi}_{n_i}^i(r_i) = \exp(-2\pi \sum_j \lambda_j \int_0^\infty y_j(1 - \widehat{\Psi}_{n_i}^i(r_i, y_j)) dy_j)$, and,

$$\widehat{\Psi}_{\mathrm{L}}^i(r_i, y_j) = \sum_{n_j\in\{\mathrm{L,N}\}} \frac{p_{n_j}^j(y_j)}{\left(1 + (N^r!)^{-\frac{1}{N^r}} l_i'' \frac{\beta_i P_j L_{n_j}^j(y_j)}{P_i L_{n_i}^i(r_i)}\right)^{S_j}}.$$

G-A Method: Using Proposition 5,

$$c^{\mathrm{SIMO-G-A}} = \sum_{i\in\mathcal{K}} \frac{2\pi\lambda_i}{(N^r - 1)!\Gamma(a)} \sum_{n_i\in\{\mathrm{L,N}\}}$$

$$\times \int_0^\infty \int_0^\infty r_i p_{n_i}^i(r_i) h^{N^r - 1} e^{-h} \gamma\left(a, b\frac{\beta_i}{P_i L_{n_i}^i(r_i) h}\right) \mathrm{d}r_i \mathrm{d}h, \tag{41}$$

where a and b are obtained by replacing $\widetilde{\Psi}_{\mathrm{ZF}}(v, y_j)$ in (25) with $\widetilde{\Psi}_{\mathrm{SIMO}}(v, y_j) = \sum_{n_j\in\mathrm{L,N}} \frac{p_{n_j}^j(y_j)}{\left(1 + P_j L_{n_j}^j(y_j)\right)}$, along with (32) and (33).

6.4.3 MISO-SDMA Systems

Another instance is when the BSs have access to CSIT in an MISO-SDMA system. Here $N^r = 1$, and $S_i = 1$, $\forall i$. We further assume that each cell of tier i serves $U_i \leq N_i^t$ UEs using ZFBF at the transmitter, see, e.g., [6], [7] for more details. Assuming a fixed transmit power, the SIR of the typical UE associated with BS x_i is

$$\mathrm{SIR}_{x_i}^{\mathrm{SDMA}} = \frac{\frac{P_i}{U_i} L_i(\|x_i\|) H_{x_i}^{\mathrm{SDMA}}}{\sum_{j\in\mathcal{K}} \sum_{x_j\in\Phi_j/x_i} \frac{P_j}{U_j} L_j(\|x_j\|) G_{x_j}^{\mathrm{SDMA}}}, \tag{42}$$

where $H_{x_i}^{\mathrm{SDMA}}$ and $G_{x_j}^{\mathrm{SDMA}}$ are both chi-squared random variables with $2(N_i^t - U_i + 1)$ and $2U_j$ DoFs, respectively [6], [14].

A-A Method: Using Proposition 4,

$$c^{\mathrm{SDMA-A-A}} = \sum_{i\in\mathcal{K}} 2\pi\lambda_i \Bigg(1 + \sum_{l_i''=0}^{N^r l_i'} (-1)^{l_i''+1}$$

$$\binom{N^r l_i'}{l_i''} \sum_{n_i \in \mathrm{L,N}} \int_0^\infty r_i p_{n_i}^i(r_i) \widehat{\Psi}_{n_i}^i(r_i) \mathrm{d}r_i \Bigg), \tag{43}$$

where $\widehat{\Psi}_{n_i}^i(r_i) = \exp(-2\pi \sum_j \lambda_j \int_0^\infty y_j(1 - \widehat{\Psi}_{n_i}^i(r_i, y_j))dy_j)$, in which,

$$\widehat{\Psi}_{n_i}^i(r_i, y_j) = \sum_{n_j \in \{\mathrm{L,N}\}} \frac{p_{n_j}^j(y_j)}{\left(1 + U_i' l_i'' \frac{\beta_i U_i P_j L_{n_j}^j(y_j)}{U_j P_i L_{n_i}^i(r_i)}\right)^{U_j}}.$$

G-A Method: Using Proposition 5, the G-A approximation is

$$c^{\mathrm{SIMO-G-A}} = \sum_{i \in \mathcal{K}} \frac{2\pi\lambda_i}{(N^r - U_i)!\Gamma(a)} \sum_{n_i \in \{\mathrm{L,N}\}}$$

$$\times \int_0^\infty \int_0^\infty r_i p_{n_i}^i(r_i) h^{N^r - U_i} e^{-h} \gamma\left(a, b \frac{\beta_i}{\frac{P_i}{U_i} L_{n_i}^i(r_i) h}\right) \mathrm{d}r_i \mathrm{d}h, \tag{44}$$

where parameters a and b are obtained by replacing $\widetilde{\Psi}_{\mathrm{ZF}}(v, y_j)$ in (25) with $\widetilde{\Psi}_{\mathrm{SDMA}}(v, y_j) = \sum_{n_j \in \mathrm{L,N}} \frac{p_{n_j}^j(y_j)}{\left(1 + \frac{P_j}{U_j} L_{n_j}^j(y_j)\right)^{U_j}}$ along with (32) and (33).

6.5 Imperfect CSIT

In practice, instead of a perfect CIST, often a delayed and/or quantized version of channel directional information (CDI) is available at the BSs. Consider the MISO-SDMA system discussed above, and assume UEs report CDI using B_i feedback bits associated with tier i. Following the same line of argument as in [75], [76], [77], we can obtain the received channel power and interference statistics. Nevertheless, based on imperfect CDI, zero-forcing beamforming is unable to completely eliminate the inter-user interference. Therefore, assuming quantization cell approximation (QCA) [75], [77], [78], the SIR of the typical UE associated with BS x_i is :

$$\mathrm{SIR}_{x_i}^{\mathrm{QSDMA}} \approx \tag{45}$$

$$\frac{\frac{P_i}{U_i} L_i(\|x_i\|) H_{x_i}^{\mathrm{SDMA}}(1 - \phi_i)}{\frac{P_i}{U_i} L_i(\|x_i\|) G_{x_i}^{\mathrm{QSDMA}} \phi_i + \sum_{j \in \mathcal{K}} \sum_{x_j \in \Phi_j / x_i} \frac{P_j}{U_j} L_j(\|x_j\|) G_{x_j}^{\mathrm{SDMA}}},$$

where $\phi_i = 2^{-\frac{B_i}{N_i^t - 1}}$ and $G_{x_i}^{\mathrm{QSDMA}}$ is an exponentially distributed random variable with unit mean and independent of $H_{x_i}^{\mathrm{SDMA}}$ and $G_{x_i}^{\mathrm{SDMA}}$ [77], [78]. Note that the SIR expression in (45) is in fact an approximation derived based on QCA. Therefore, assuming exponential distribution for random variable, $G_{x_i}^{\mathrm{QSDMA}}$, highly relies on QCA and may become inaccurate if this assumption does not hold. Nevertheless, as our simulations also suggest, the QCA assumption provides a high level of accuracy, and therefore (45) is rather a close approximation.

For a system with imperfect CDIR, we obtain the outage probability using A-A and G-A methods.

A-A Method:

Using Proposition 4,

$$c^{\mathrm{QSDMA-A-A}} = \sum_{i \in \mathcal{K}} 2\pi\lambda_i \Bigg(1 + \sum_{l_i''=0}^{N^r l_i'} (-1)^{l_i''+1}$$

$$\binom{N^r l_i'}{l_i''} \sum_{n_i \in \mathrm{L,N}} \int_0^\infty \frac{r_i p_{n_i}^i(r_i) \widehat{\Psi}_{n_i}^i(r_i)}{1 + U_i' l_i'' \frac{P_i}{U_i} L_{n_i}^i(r_i) \phi_i} \mathrm{d}r_i \Bigg), \tag{46}$$

where $\widehat{\Psi}_{n_i}^i(r_i) = \exp(-2\pi \sum_j \lambda_j \int_0^\infty y_j(1 - \widehat{\Psi}_{n_i}^i(r_i, y_j))dy_j)$, in which,

$$\widehat{\Psi}_{n_i}^i(r_i, y_j) = \sum_{n_j \in \{\mathrm{L,N}\}} \frac{p_{n_j}^j(y_j)}{\left(1 + U_i' l_i'' \frac{\beta_i}{1 - \phi_i} \frac{U_i P_j L_{n_j}^j(y_j)}{U_j P_i L_{n_i}^i(r_i)}\right)^{U_j}}.$$

G-A Method:

Using Proposition 5, the G-A approximation is

$$c^{\mathrm{QSDMA-G-A}} = \sum_{i \in \mathcal{K}} \frac{2\pi\lambda_i}{(N^r - U_i)!\Gamma(a)} \sum_{n_i \in \{\mathrm{L,N}\}}$$

$$\times \int_0^\infty \int_0^\infty \frac{r_i p_{n_i}^i(r_i) h^{N^r - U_i} e^{-h}}{1 + \frac{P_i}{U_i} L_{n_i}^i(r_i) \phi_i} \gamma\left(a, b \frac{\frac{\beta_i}{(1 - \phi_i)}}{\frac{P_i}{U_i} L_{n_i}^i(r_i) h}\right) \mathrm{d}r_i \mathrm{d}h, \tag{47}$$

where a and b are obtained by replacing $\widetilde{\Psi}_{\mathrm{ZF}}(v, y_j)$ in (25) with $\widetilde{\Psi}_{\mathrm{SDMA}}(v, y_j) = \sum_{n_j \in \mathrm{L,N}} \frac{p_{n_j}^j(y_j)}{\left(1 + \frac{P_j}{U_j} L_{n_j}^j(y_j)\right)^{U_j}}$ along with (32) and (33).

From the above analysis, one can see that an imperfect CSIT increases the SIR threshold from β_i to $\frac{\beta_i}{1 - \phi_i}$. Imperfect CSIT also creates extra interference—inter-user interference— but the level of this extra interference is reduced by increasing B_i.

7 Simulations and Numerical Analysis

We first evaluate the accuracy of the proposed approximations of the coverage probability. We then study the effects of various system parameters on the coverage probability as well as area spectral efficiency (ASE) to gain insight on the effects of densification, multiplexing gains, and propagation environment.

The simulation results are based on the Monte Carlo simulation, where 40,000 snap-shots are independently simulated and averaged. In each snap-shot, we randomly create BSs based on the given densities in a disk with radius of 10,000 units. The fading matrices are then randomly generated for each snap-shot based on a Rayleigh fading distribution. The LOS/NLOS path-loss for each BS is also specified based on the probabilistic model in (3). System parameters are set as: $P_1 = 25$ W, $P_2 = 1$ W, $N_1^t = 16$, $N_2^t = 8$, $N^r = 8$, $\beta_1 = 5$, $\beta_2 = 2.5$, $D_0^1 = 36$, $D_0^2 = 9$, $D_1^1 = 48$, $D_1^2 = 18$ meters, and $\phi_{\mathrm{L}}^i = \phi_{\mathrm{N}}^i = 1$.

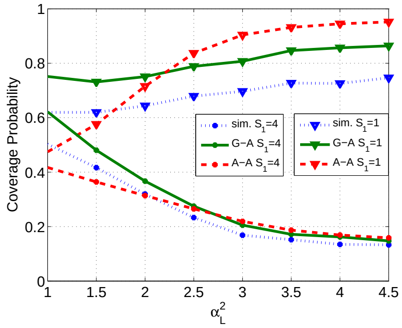

Fig. 4. Coverage probability *vs.* α_L^2, where $\lambda_1 = 10^{-4}$, $\lambda_2 = 10^{-3}$, $S_2 = 2$, $\alpha_{\rm L}^1 = 2.09$, $\alpha_{\rm N}^1 = 3.75$, and $\alpha_{\rm N}^2 = 4.75$.

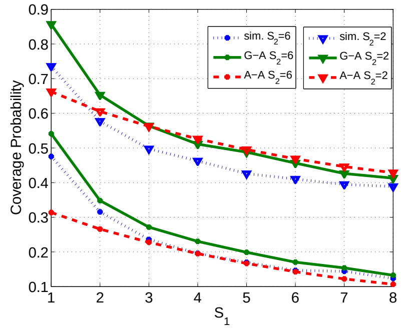

Fig. 5. Coverage probability *vs.* S_1, where $\lambda_1 = 10^{-4}$, $\lambda_2 = 10^{-3}$, $\alpha_{\rm L}^1 = 2.09$, $\alpha_{\rm N}^1 = 3.75$, $\alpha_{\rm L}^1 = 1.5$, and $\alpha_{\rm N}^2 = 4.75$.

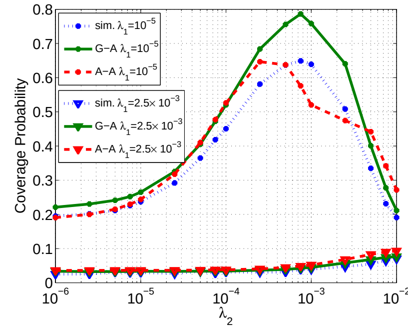

Fig. 6. Coverage probability *vs.* λ_2, where $S_1 = 4$, $S_2 = 2$, $\alpha_{\rm L}^1 = 2.09$, $\alpha_{\rm N}^1 = 3.75$, $\alpha_{\rm L}^1 = 1.5$, and $\alpha_{\rm N}^2 = 4.75$.

7.1 Accuracy of A-A and G-A

Fig. 4 shows the coverage probability vs. α_L^2. The level of accuracy achieved by $c^{\rm G-A}$ is shown to be higher than that of $c^{\rm A-A}$. The inaccuracy gap induced by $c^{\rm A-A}$ is almost twice as much of $c^{\rm G-A}$.[3] G-A is also shown to act as an upper-bound on the actual coverage performance with an almost fixed inaccuracy gap. A-A, however, results in a varying inaccuracy gap depending on the value of α_L.

Fig. 5 shows the coverage probability vs. S_1 for $S_2 = 2$. For $S_1 \geq 4$, both $c^{\rm A-A}$ and $c^{\rm G-A}$ are shown close to the actual value. The larger the S_2, the higher the accuracy of $c^{\rm A-A}$. However, for $S_1 < 4$, the A-A becomes less accurate and fails to follow the actual coverage probability. In contrast, $c^{\rm G-A}$ preserves a reasonable accuracy for all ranges of multiplexing gains, and is able to follow the variations in the actual coverage probability. Furthermore, G-A is shown to always act as an upper-bound on the coverage probability, while A-A alternates between being upper- and lower-bounded.

Fig. 6 shows the coverage probability vs. λ_2, where $(S_1 = 4, S_2 = 2)$. The density is measured as the number of nodes per square meter. We consider two choices of sparse $(\lambda_1 = 10^{-5})$ and moderately dense $(\lambda_1 = 2.5 \times 10^{-3})$. For $\lambda_1 = 2.5 \times 10^{-3}$, both $c^{\rm A-A}$ and $c^{\rm G-A}$ are shown very close to the actual coverage probability. For $\lambda_1 = 10^{-5}$, while acting as an upper-bound, $c^{\rm G-A}$ closely follows the coverage probability and accurately predicts the best achieved coverage probability. For A-A, like previous cases, $c^{\rm A-A}$ alternates between being upper- and lower-bounded, and is also unable to predict the density for which the highest coverage probability is achieved. The above results show that $c^{\rm G-A}$ provides a better approximation than that of $c^{\rm A-A}$.

3. Fig. 4 shows that Alzer approximation is neither an upper-bound nor a lower-bound on the coverage probability, while the Alzer method basically provides an upper-bound when it is used for SISO systems under Nakagami-type fading, MISO-SDMA and SIMO communication systems, and also in mmWave communication systems with directional antennas [53], [56], [57]. By Proposition 4, the obtained coverage probability is in fact a summation over indices of multiplexing gains, where depending on the multiplexing gains, some terms may adopt a negative signs. Therefore, although the Alzer's inequality provides an upper-bound for each data stream, summing up the upper-bounds results in an approximation based on the bounds provided by the Alzer method.

7.2 Coverage Probability

7.2.1 *Impact of α_L^2*

Fig. 4 shows that increasing α_L^2 may increase/decrease the coverage probability, depending on the value of multiplexing gain, S_1. For $(S_1 = 1, S_2 = 2)$, increasing α_L^2 improves the coverage probability. In this case, the LOS signals in Tier 2 are weakened, while the ICI is increased. These make it difficult to decode $S_2 = 2$ transmitted data streams. Thus, the serving BS will most likely be selected from Tier 1. Similarly, for a large enough α_L^2, successful decoding of $S_1 = 1$ data stream is easier than that of $S_2 = 2$, and hence the serving BS is most likely selected from Tier 1. In contrast, for $(S_1 = 4, S_2 = 2)$, increasing α_L^2 degrades the coverage performance, because the serving BS is most likely selected from Tier 2, as successful decoding of $S_2 = 2$ data streams is much more likely than that of $S_1 = 4$.

7.2.2 *Impact of Multiplexing Gains*

To study the impact of multiplexing gain, Fig. 5 presents the coverage probability vs. S_1. Increasing S_1 is shown to decrease the coverage probability, because the larger the multiplexing gain, the less probable the typical UE can simultaneously decode all data streams. Furthermore, increasing S_1 also increases the power of ICI on each data stream. In general, system diversity is shown to provide a higher coverage than that of system multiplexing.

This finding can be substantiated by an analysis. We use the following upper-bound (see Appendix G) on the coverage probability

$$c^{\rm ZF-FC} \leq \left(\int_0^\infty \widetilde{\Psi}(v){\rm d}v\right) 2\pi \sum_{i\in\mathcal{K}} \frac{\lambda_i P_i \overline{L}_i}{\beta_i}\Big(\frac{N^r+1}{S_i} - 1\Big), \quad (48)$$

where $\overline{L}_i = \int_0^\infty r_i \mathbb{E}_{L_i(r_i)}[L_i(r_i)]{\rm d}r_i$, and $\widetilde{\Psi}(v)$ is given in (24). In (48), $\int_0^\infty \widetilde{\Psi}(v){\rm d}v$ represents the effect of interference that is a decreasing function of multiplexing gain S_i.[4] Moreover,

4. To see this, one needs to show that function $\widetilde{\Psi}_{\rm ZF}(v, y_j)$ defined in (25) is a decreasing function of S_j. Note that $\widetilde{\Psi}_{\rm ZF}(v, y_j) \propto \left(1 + \frac{P_j}{S_j} L_{n_j}^j(y_j)\right)^{-S_j}$. Therefore, the differentiation of the logarithm function in the right-hand-side with respect to S_j (assuming that S_j is continues) is always negative, i.e., $\frac{\partial}{\partial S_j} \log\left(1 + \frac{P_j}{S_j} L_{n_j}^j(y_j)\right)^{-S_j} \leq 0$.

$\frac{N^r+1}{S_i}-1$ is also related to the effective DoF of each data stream, which is a decreasing function of S_i. Therefore, the upper-bound (48) of the coverage probability declines by increasing S_i. The derived upper-bound is shown to provide insights on the impact of multiplexing gain of the coverage performance. However, as it is not the tightest upper-bound, the actual decline rate of the coverage probability due to the increase of S_i might be slightly different from that suggested by (48). A more accurate upper-bound can be obtained via Chebyshev's inequality. However, it requires the evaluation of second-order statistics of the accumulated data rate across data streams.

7.2.3 Impact of Densification

To study the impact of densification, Fig. 6 plots the coverage probability vs. λ_2. For $\lambda_1 = 10^{-5}$, the highest coverage probability is achieved when λ_2 is around 10^{-3}. Fig. 6 also shows that for $\lambda_2 < 10^{-3}$, the coverage probability can be improved by increasing the density of BSs in Tier 2. In such cases, although excessive ICI is created due to densification, many of the Tier-2 BSs are close enough to the typical UE to have an LOS path-loss. Fig. 6 shows that the excessive ICI is apparently dominated by the existence of many strong LOS Tier-2 BSs suitable for association. Furthermore, association with a BS in Tier 2 might be preferred to one in Tier 1as successful decoding of all $S_2 = 2$ data streams is more probable than that of $S_1 = 4$ data streams.

For $\lambda_2 > 10^{-3}$, increasing the density of Teir 2 might lead to a significant decline of the coverage probability. This is attributed to the growth of ICI, especially caused by many LOS interferer BSs in Tier 2. In this case, even association with a very close LOS BS cannot compensate the ICI growth. In this case, Tier 1 remains less qualified for association due to its high multiplexing gain. It is further shown in Fig. 6 that the coverage probability is substantially degraded by increasing λ_1 to 2.5×10^{-3}. This is due to the increase of ICI as well as Tier 1's high multiplexing gain.

The bell-shaped curve observed in Fig. 6 can also be explained as follows. In Appendix H, we derive the following upper-bound on the coverage probability:

$$c^{\mathrm{ZF-FC}} \le \sum_{i\in\mathcal{K}} 2\pi\lambda_i \int_0^\infty r\mathbb{E}_{L_i(r)}\exp\Big\{-2\pi\sum_j \lambda_j \int_0^\infty \mathbb{E}_{L_j(y)} \Omega_{i,j}\Big(\frac{P_iS_jL_i(r)}{P_jS_iL_j(y)\beta_i}\Big)dy\Big\}\mathrm{d}r, \tag{49}$$

where

$$\Omega_{i,j}\Big(\frac{P_iS_jL_i(r_i)}{P_jS_iL_j(y)\beta_i}\Big) = y\overline{F}_{\frac{G_j^{\mathrm{ZF}}}{H_{i,\min}^{\mathrm{ZF}}}}\Big(\frac{P_iS_jL_i(r_i)}{P_jS_iL_j(y)\beta_i}\Big), \tag{50}$$

and $\overline{F}_{\frac{G_j^{\mathrm{ZF}}}{H_{i,\min}^{\mathrm{ZF}}}}(.)$ is the CCDF of random variable $\frac{G_j^{\mathrm{ZF}}}{H_{i,\min}^{\mathrm{ZF}}}$, the exact shape of which is not important for our purpose. As shown in (49), by increasing λ_i, the coverage probability increases proportionally by a multiplicative scale, λ_i, while it is simultaneously decreased exponentially. This conflicting behavior suggests that by densification, depending on the system parameters, one of the above phenomena becomes dominant and then the coverage probability can either grow or decline. By differentiating (49) with respect to the densities λ_i and letting the resultants equal to 0, a set of the following K equations are obtained:

$$\int_0^\infty r\mathbb{E}_{L_i(r)}\Bigg[e^{-2\pi\sum_j\lambda_j\int_0^\infty \mathbb{E}_{L_j(y)}\Omega_{i,j}\left(\frac{P_iS_jL_i(r)}{P_jS_iL_j(y)\beta_i}\right)dy} \times\Bigg(1-2\pi\lambda_i\int_0^\infty \mathbb{E}_{L_j(y)}\Omega_{i,i}\Big(\frac{L_i(r)}{L_j(y)\beta_i}\Big)\Bigg)\Bigg]\mathrm{d}r = 0, \quad \forall i\in\mathcal{K}.$$

This suggests that there exist a set of densities maximizing the coverage probability.

7.2.4 Impact of Interference Correlation

Our analysis in this paper is based on FC assumption. To better understand the utility of this approximation, we compare the coverage probability under FC assumption with a manufactured scenario whereby for each data stream l_i, K independent sets of interferers denoted by $\Phi_j^{l_i}$ with given density λ_j are produced. To highlight this approach, we call it No-Correlation (NC) assumption. Similarly to Propositions 4 and 5, one can estimate the coverage probability via A-A and A-G methods, respectively.

Corollary 3: Define $S_i' = ((N^r-S_i+1)!)^{-\frac{1}{(N^r-S_i+1)}}$. Under NC assumption and based on the A-A method, the coverage probability is approximated as

$$c^{\mathrm{A-A}} = \sum_{i\in\mathcal{K}} 2\pi\lambda_i \int_0^\infty r_i \sum_{n_i\in\mathrm{L,N}} p_{n_i}^i(r_i)\Bigg(\sum_{l_i''=1}^{N^r-S_i+1}\binom{N^r-S_i+1}{l_i''} \times(-1)^{l_i''+1}\widehat{\Psi}_{n_i}^i(r_i)\Bigg)^{S_i}\mathrm{d}r_i, \tag{51}$$

where $\widehat{\Psi}_{n_i}^i(r_i)$ is as given in Proposition 4.

Proof: See Appendix I. ∎

Corollary 4: Under NC assumption, and based on the G-A method, the coverage probability is approximated as

$$c^{\mathrm{G-A}} = \sum_{i\in\mathcal{K}} 2\pi\lambda_i \int_0^\infty r_i \sum_{n_i\in\{\mathrm{L,N}\}} p_{n_i}^i(r_i) \times\Bigg(\int_0^\infty \frac{h^{N^r-S_i}e^{-h}}{(N^r-S_i)!\Gamma(a)}\gamma\left(a, b\frac{\beta_i}{\frac{P_i}{S_i}L_{n_i}^i(r_i)h}\right)\mathrm{d}h\Bigg)^{S_i}\mathrm{d}r_i, \tag{52}$$

where $\gamma(a,bx)$ is the CCDF of random variable $\mathrm{Gamma}(a,b)$.

Proof: See Appendix J. ∎

Fig. 7 shows the coverage probability vs. β_1. The FC assumption is shown to provide a much higher accuracy than NC assumption. One may assume that the intrinsic received diversity gain in adopting NC assumption overestimates the coverage probability compared to the FC assumption. Surprisingly, the opposite is observed in Fig. 7, showing that the coverage probability under NC is much smaller than that of FC. This is due mainly to the existence of LOS component, as in the NC case for each data stream, the typical UE is interfered with by a new set of K independent PPP interferers. Therefore, it is highly likely for the typical UE to have a larger number of LOS-dominated interfering

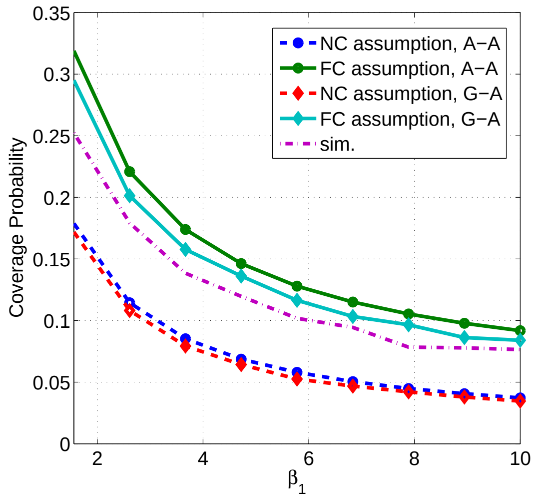

Fig. 7. Coverage probability *vs.* β_1, where $S_1 = 2$, $S_2 = 6$, $\beta_2 = 2.5$, $\lambda_1 = 10^{-4}$, and $\lambda_2 = 10^{-3}$.

links from the BSs. In contrast, under the FC assumption across all data streams, the very same set of K independent PPP interferes are interfering with the typical UE. Compared to the FC assumption, this results in a significantly higher interference and therefore a much lower coverage probability under the NC assumption. In other words, the improved receive diversity due to no-correlated interference is compromised by a larger number of LOS interfering links.

7.2.5 Nonhomogeneous Path-Loss Model

We study the non-homogeneous path-loss scenario as described in Section 6. Fig. 8 shows the corresponding coverage performance vs. λ_2 with the same system parameter considered in Fig. 6. G-A is shown to provide a higher level of accuracy than that of A-A. For $\lambda_1 = 2.5 \times 10^{-3}$ and $5 \times 10^{-3} < \lambda_2 < 10^{-2}$, the coverage probability obtained by A-A is not reliable. Nevertheless, G-A preserves a consistent accuracy and robustness. This justifies G-A's higher numerical complexity. Densification in Tier 2 is also shown to improve the coverage probability. This is in contrast with what Fig. 6 shows. This can be explained by noting that under the non-homogenous scenario, the path-loss exponents in Tier 1 are increased, reducing the aggregated interference. Therefore, even receiving a weaker signal power per each data stream is enough to overcome the impact of the interference and establish a communication link with a BS in Tier 2. On the other hand, as in the case of Fig. 6, densification in Tier 1 lowers the coverage performance in a non-homogeneous path-loss environment. In this case, larger path-loss exponents do not improve the coverage probability because setting $S_1 = 4$ makes it increasingly unlikely for a typical user to be associated with a BS in Tier 1.

7.3 Impact of Imperfect CSIT

In Fig. 11, we investigate the impact of imperfect CSIT on the coverage performance based on the derivations in Section 6.5 using QCA. As shown in Fig. 11, the QCA

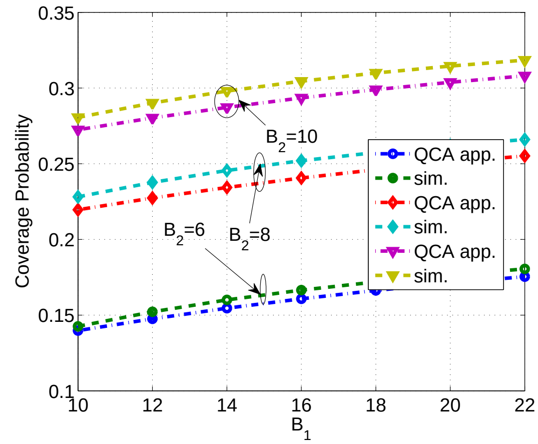

Fig. 11. Coverage probability *vs.* B_1, where $\lambda_1 = 10^{-3}$, $\lambda_2 = 10^{-2}$, $U_1 = 10$, and $U_2 = 2$. The analytical result is based on G-A approximation.

approximation closely follows the actual coverage performance. Note that for clarity we only consider the G-A approximation in this simulation.

7.4 Area Spectral Efficiency (ASE)

Area spectral efficiency (ASE) of the network is often considered as a crucial performance metric in cellular communication systems. ASE is defined as $\mathrm{ASE}^{\mathrm{ZF}} = \sum_i \lambda_i S_i c_i^{\mathrm{ZF}} \log(1+\beta_i)$ nat/s/Hz/unit area [6], [7], [33], where c_i^{ZF} is the coverage probability from Tier i. Note that ASE is linearly proportional to the multiplexing gain S_i, but there is no guarantee that increasing the multiplexing gains improves ASE, as it may degrade the coverage probability.

Here we consider two systems: system 1 (SYS1) wherein both LOS and NLOS components exist, and system 2 (SYS2) which has non-homogeneous path-loss model in which all BSs are subject to the NLOS component. The density of BSs in both SYS1 and SYS2 are the same.

7.4.1 Impact of α_L^2, and Multiplexing Gain

Fig. 9 shows the impact of near-field path-loss exponent in Tier 2, α_L^2, on the ASE. As expected, in SYS2 by increasing α_L^2, the ASE does not change. This is because in the non-homogenous path-loss model, LOS/NLOS path-loss exponents are considered equal in each tier, and different across different tiers. Increasing $S_1 = 1$ to $S_1 = 4$ does not change ASE in both SYS1 and SYS2. Thus, it may not be necessarily suitable to increase the multiplexing gains, as it does not directly improve the ASE while it may degrade coverage performance. Fig. 9 also shows that the ASE in SYS1 is higher than that in SYS2 and a higher ASE gain is achieved for smaller α_L^2. Therefore, unlike the cases with all NLOS links, the LOS links can improve the ASE.

7.4.2 Impact of Densification and Multiplexing Gain

Fig. 10 plots ASE vs. S_1. In general, G-A is shown to be more accurate than A-A. Further, the figure shows that the ASE is slightly reduced by increasing S_1. Recall the coverage performance from Fig. 5, showing that the coverage probability is decreased by increasing multiplexing gains. Thus,

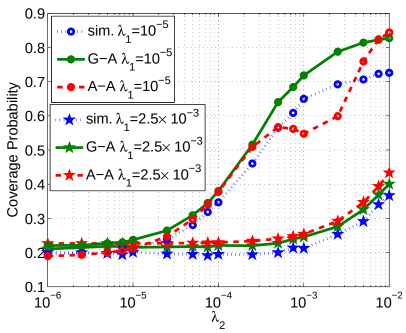

Fig. 8. Coverage probability *vs.* λ_2, where $S_1 = 4$, $S_2 = 2$, $\alpha_1 = 2.09$, and $\alpha_2 = 4.75$.

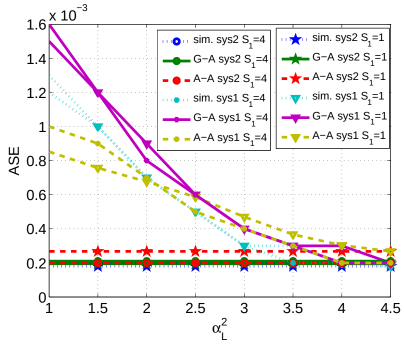

Fig. 9. ASE *vs.* α_L^2, where $\lambda_1 = 10^{-4}$, $\lambda_2 = 10^{-3}$, $S_2 = 2$, $\alpha_L^1 = 2.09$, $\alpha_N^1 = 3.75$, and $\alpha_N^2 = 4.75$.

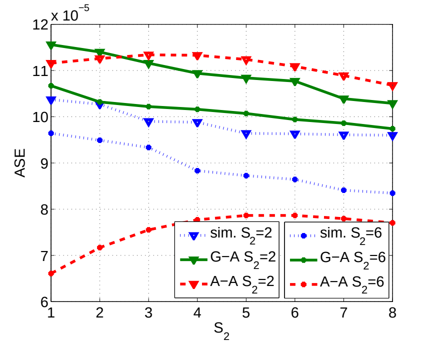

Fig. 10. ASE *vs.* S_1, where $\lambda_1 = 10^{-4}$, $\lambda_2 = 10^{-3}$, $\alpha_L^1 = 2.09$, $\alpha_N^1 = 3.75$, $\alpha_L^1 = 1.5$, and $\alpha_N^2 = 4.75$.

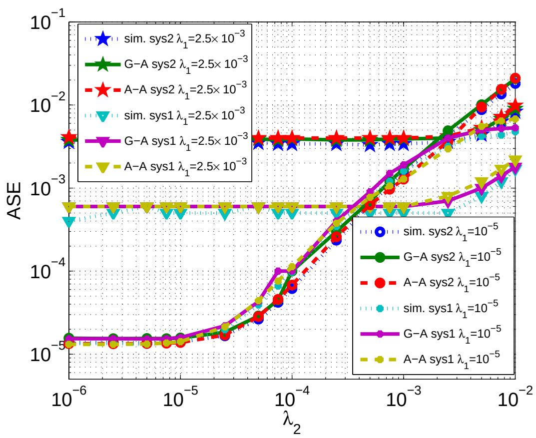

Fig. 12. ASE *vs.* λ_2, where $S_1 = 4$, $S_2 = 2$, $\alpha_L^1 = 2.09$, $\alpha_N^1 = 3.75$, $\alpha_L^1 = 1.5$, and $\alpha_N^2 = 4.75$.

we conclude that in many cases adopting a diversity only system (see Section 6) is justifiable.

Fig. 12 plots ASE vs. λ_2 for $S_1 = 4$ and $S_2 = 2$. Regardless of the multiplexing gains and the density of Tier 1, Fig. 12 shows that increasing λ_2 improves the ASE in both systems. One should also note that densification of Tier 1 may not necessarily improve the ASE. In fact, in SYS2, ASE is degraded by increasing the density of Tier 1. Furthermore, in SYS1, for $\lambda_2 > 5 \times 10^{-3}$, growing the density of Tier 1 improves the ASE. In contrast, for $\lambda_2 < 5 \times 10^{-3}$, the ASE is not related to the density of Tier 1. For this setting ($\lambda_2 > 5 \times 10^{-3}$), the rate of ASE increase by increasing λ_2 is smaller for higher Tier 1's density. This is consistent with the observation made in Fig. 6, where for $S_1 = 4$, densification in Tier 1 lowers coverage performance.

Note that for $\lambda_2 > 5 \times 10^{-5}$, $\lambda_1 = 2.5 \times 10^{-3}$, SYS1 outperforms SYS2. This suggests that the existence of the LOS component has a positive effect on the ASE. In contrast, for $\lambda_2 < 5 \times 10^{-5}$, ASE in SYS1 is, in fact, smaller than that in SYS2 due to the LOS component.

8 Conclusions

For open-loop multi-stream MIMO-ZFBF communications in random networks subject to LOS/NLOS propagation, we evaluated the coverage probability. Adopting the tool of stochastic geometry, we derived two easy-to-compute approximations of the coverage probability, A-A and G-A methods, as the function of densities of tiers, multiplexing gains, LOS/NLOS parameters, the number of receiver antennas, and the number of tiers. Our extensive simulation and numerical evaluations revealed that G-A is more accurate than A-A. Compared to A-A, G-A is also more robust to various system parameters and can accurately predict the best density responsible for the peak of the coverage probability. We therefore recommend its use if one wants to investigate other aspects of the system or carry out system design. Our results also showed that, under certain scenarios, the existence of LOS mode can render perceivable ASE performance boost over the case where all communication links are in NLOS mode. To achieve this, one must judiciously choose the density of BSs.

We also studied the cross-stream ICI correlation. Our analysis showed that in the MIMO multiplexing system, the ICI is highly correlated across data streams. This finding can substantially ease the performance evaluation of multi-stream systems, as shown in this paper.

The analytical results in this paper can also facilitate analysis of mmWave multiplexing for which researchers commonly focused on the stream-level performance evaluation instead of the link-level performance [56], [57].

References

[1] M. G. Khoshkholgh and V. C. M. Leung, "Impact of LOS/NLOS propagation on the coverage performance of multi-stream MIMO-ZFBF cellular downlink," in *IEEE 86th Vehicular Technology Conference (VTC-Fall)*, Sept. 2017.

[2] J. G. Andrews, S. Buzzi, W. Choi, S. V. Hanly, A. Lozano, A. C. K. Soong, and J. C. Zhang, "What will 5G be?," *IEEE Journal on Selected Areas in Communications*, vol. 32, no. 6, pp. 1065–1082, June 2014.

[3] F. Boccardi, R. W. Heath, A. Lozano, T. L. Marzetta, and P. Popovski, "Five disruptive technology directions for 5G," *IEEE Communications Magazine*, vol. 54, no. 2, pp. 74–80, Feb. 2014.

[4] H. S. Dhillon, R. K. Ganti, F. Baccelli, and J. G. Andrews, "Modeling and analysis of K-tier downlink heterogeneous cellular networks," *IEEE Journal on Selected Areas in Communications*, vol. 30, no. 3, pp. 550–560, Apr. 2012.

[5] J. G. Andrews, F. Baccelli, and R. K. Ganti, "A tractable approach to coverage and rate in cellular networks," *IEEE Transactions on Communications*, vol. 59, no. 11, pp. 3122–3134, Nov. 2011.

[6] H. S. Dhillon, M. Kountouris, and J. G. Andrews, "Downlink MIMO hetnets: Modeling, ordering results and performance analysis," *IEEE Transactions on Wireless Communications*, vol. 12, no. 10, pp. 5208–5222, Oct. 2013.

[7] C. Li, J. Zhang, J. G. Andrews, and K. B. Letaief, "Success probability and area spectral efficiency in multiuser MIMO HetNets," *IEEE Transactions on Communications*, vol. 64, no. 4, pp. 1544–1556, Apr. 2016.

[8] M. Haenggi, J. G. Andrews, F. Baccelli, O. Dousse, and M. Franceschetti, "Stochastic geometry and random graphs for the analysis and design of wireless networks," *IEEE Journal on Selected Areas in Communications*, vol. 27, no. 7, pp. 1029–1046, Sept. 2009.

[9] H. ElSawy, A. Sultan-Salem, and M.-S. Alouini, "Modeling and analysis of cellular networks using stochastic geometry: A tutorial," *IEEE Communications Surveys & Tutorials*,, vol. 19, no. 1, pp. 167–203, Firstquarter 2017.

[10] F. Baccelli and B. Blaszczyszyn, *Stochastic geometry and wireless networks, vol. II*. NOW: Foundations and Trends in Networking, 2009, vol. 3, no. 2.

[11] W. Lu and M. D. Renzo, "Stochastic geometry modeling of cellular networks: Analysis, simulation and experimental validation," in *Proceedings of the 18th ACM International Conference on Modeling, Analysis and Simulation of Wireless and Mobile Systems (MSWiM's 15)*, Nov. 2015, pp. 179–188, [Online]. http://arxiv.org/abs/1506.03857.

[12] A. Guo and M. Haenggi, "Spatial stochastic models and metrics for the structure of base stations in cellular networks," *IEEE Transactions on Wireless Communications*, vol. 12, no. 11, pp. 5800–5812, Nov. 2013.

[13] J. Liu, M. Sheng, L. Liu, and J. Li, "Effect of densification on cellular network performance with bounded pathloss model," *IEEE Communications Letters*, vol. 21, no. 2, pp. 346–349, Feb. 2017.

[14] M. G. Khoshkholgh and V. C. M. Leung, "Coverage analysis of max-sir cell association in hetnets under nakagami fading," *IEEE Trans. Veh. Technol.*, vol. 67, no. 3, pp. 2420–2438, Mrc. 2018.

[15] X. Zhang and J. G. Andrews, "Downlink cellular network analysis with multi-slope path loss models," *IEEE Transactions on Communications*, vol. 63, no. 5, pp. 1881–1894, May 2015.

[16] 3GPP, "Technical specification group radio access network; evolved universal terrestrial radio access (E-UTRA); further advancements for E-UTRA physical layer aspects (Release 9). TR 36.814," 2010.

[17] J. Arnau, I. Atzeni, and M. Kountouris, "Downlink cellular network analysis with LOS/NLOS propagation and elevated base stations," *IEEE Trans. Wireless Commun.*, vol. 17, no. 1, pp. 142–156, Jan. 2018.

[18] C. Galiotto, N. K. Pratas, N. Marchetti, and L. Doyle, "Effect of LOS/NLOS propagation on 5G ultra-dense networks," *Computer Networks*, vol. 120, pp. 126–140, June 2017.

[19] J. G. Andrews, X. Zhang, G. D. Durgin, and A. K. Gupta, "Are we approaching the fundamental limits of wireless network densification?," *IEEE Communications Magazine*, vol. 54, no. 10, pp. 184–190, Oct. 2016.

[20] C. S. Chen, V. M. Nguyen, and L. Thomas, "On small cell network deployment: A comparative study of random and grid topologies," in *Proc. IEEE Veh. Technol. Conf. (VTC Fall)*, 2012.

[21] M. D. Renzo, W. Lu, and P. Guan, "The intensity matching approach: A tractable stochastic geometry approximation to system-level analysis of cellular networks," *IEEE Transactions on Wireless Communications*, vol. 15, no. 9, pp. 5963–5983, Sept. 2016.

[22] R. V. T. Bai and R. W. Heath Jr., "Analysis of blockage effects on urban cellular networks," *IEEE Transactions on Wireless Communications*, vol. 13, no. 9, pp. 5070–5083, Sept. 2014.

[23] M. Taranetz, R. W. Heath Jr. and M. Rupp, "Analysis of urban two-tier heterogeneous mobile networks with small cell partitioning," *IEEE Transactions on Wireless Communications*, vol. 15, no. 10, pp. 7044–2613, Oct. 2016.

[24] V. M. Nguyen and M. Kountouris, "Performance limits of network densification," *IEEE Journal on Selected Areas in Communications*, vol. 35, no. 6, pp. 1294–1308, June 2017.

[25] M. Ding, P. Wang, D. Lopez-Perez, G. Mao, and Z. Lin, "Performance impact of LoS and NLoS transmissions in dense cellular networks," *IEEE Transactions on Wireless Communications*, vol. 15, no. 3, pp. 2365–2380, Mar. 2016.

[26] T. Ding, M. Ding, Z. L. G. Mao, D. Lopez-Perez, and A. Y. Zomaya, "Uplink performance analysis of dense cellular networks with LoS and NLoS transmissions," *IEEE Transactions on Wireless Communications*, vol. 16, no. 4, pp. 2601–2613, Apr. 2017.

[27] T. T. Lam, M. D. Renzo, and J. P. Coon, "System-level analysis of SWIPT MIMO cellular networks," *IEEE Commun. Let.*, vol. 20, no. 10, pp. 2015–2018, Oct. 2016.

[28] M. D. Renzo, "Stochastic geometry modeling and analysis of multi-tier millimeter wave cellular networks," *IEEE Trans. Wireless Commun.*, vol. 14, no. 9, pp. 5038–5057, Sept. 2015.

[29] M. D. Renzo and W. Lu, "System-level analysis and optimization of cellular networks with simultaneous wireless information and power transfer: Stochastic geometry modeling," *IEEE Trans. Veh. Technol.*, vol. 66, no. 3, pp. 2251–2275, Mrc. 2017.

[30] M. G. Khoshkholgh, K. G. Shin, K. Navaie, and V. C. M. Leung, "Coverage performance in multi-stream MIMO-ZFBF heterogeneous networks," *IEEE Trans. Veh. Technol.*, vol. 66, no. 8, pp. 6801–6818, Aug. 2017.

[31] M. G. Khoshkholgh, K. Navaie, K. g. Shin, and V. Leung, "Coverage performance of MIMO-MRC in heterogeneous networks: a stochastic geometry perspective," in *IEEE 84th Vehicular Technology Conference (VTC-Fall)*, Sept. 2016.

[32] M. G. Khoshkholgh and V. C. M. Leung, "On the performance of MIMO-SVD multiplexing systems in hetnets: A stochastic geometry perspective," *IEEE Trans. Veh. Technol.*, vol. 66, no. 9, pp. 8163–8178, Sept. 2017.

[33] ——, "Closed-form approximations for coverage probability of multistream MIMO-ZFBF receivers in HetNets," *IEEE Trans. Veh. Technol.*, vol. 66, no. 11, pp. 9862–9879, Nov. 2017.

[34] M. G. Khoshkholgh, K. Navaie, K. G. Shin, and V. C. M. Leung, "Cell association in dense heterogeneous cellular networks," *IEEE Trans. Mobile Computing*, vol. 17, no. 5, pp. 1019–103, May 2018.

[35] Y. Lin, W. Bao, W. Yu, and B. Liang, "Optimizing user association and spectrum allocation in hetnets: A utility perspective," *IEEE JSAC*, vol. 33, no. 6, pp. 1025–1039, June 2015.

[36] K. Son, S. Chong, and G. D. Veciana, "Dynamic association for load balancing and interference avoidance in multi-cell networks kyuho son, student member," *IEEE Trans. Wireless Commun.*, vol. 8, no. 7, pp. 3566–3576, Jul. 2009.

[37] A. M. Hunter, J. G. Andrews, and S. Weber, "Transmission capacity of ad hoc networks with spatial diversity," *IEEE Trans. Wireless Commun.*, vol. 7, no. 12, pp. 5058–5071, Dec. 2008.

[38] M. Kountouris and J. G. Andrews, "Downlink SDMA with limited feedback in interference-limited wireless networks," *IEEE Trans. Wireless Commun.*, vol. 11, no. 8, pp. 2730–2741, Aug. 2012.

[39] V. Chandrasekhar, M. Kountouris, and J. G. Andrews, "Coverage in multi-antenna two-tier networks," *IEEE Trans. Wireless Commun.*, vol. 8, no. 10, pp. 5314–5327, Oct. 2009.

[40] A. K. Gupta, H. S. Dhillon, S. Vishwanath, and J. G. Andrews, "Downlink multi-antenna heterogeneous cellular network with load balancing," *IEEE Trans. Commun.*, vol. 62, no. 11, pp. 4052–4067, Nov. 2014.

[41] U. Schilcher, S. Toumpis, M. Haenggi, A. Crismani, G. Brandner, and C. Bettstetter, "Interference functionals in poisson networks," *IEEE Trans. Inf. Theory*, vol. 62, no. 1, pp. 370–383, Jan. 2016.

[42] A. Shojaeifard, K. A. Hamdi, E. Alsusa, D. K. C. So, and J. Tang, "Exact SINR statistics in the presence of heterogeneous interferers," *IEEE Trans. Inf. Theory*, vol. 61, no. 12, pp. 6759–6773, Dec. 2015.

[43] R. Tanbourgi, H. S. Dhillon, and F. K. Jondral, "Analysis of joint transmit-receive diversity in downlink MIMO heterogeneous cellular networks," *IEEE Transactions on Wireless Communications*, vol. 14, no. 12, pp. 6695–6709, Jul. 2015.

[44] M. D. Renzo and P. Guan, "Stochastic geometry modeling, system-level analysis and optimization of uplink heterogeneous cellular networks with multi-antenna base stations," *IEEE Trans. Commun.*, vol. 64, no. 6, pp. 2453–2476, June 2016.

[45] ——, "Stochastic geometry modeling of coverage and rate of cellular networks using the Gil-Pelaez inversion theorem," *IEEE Commun. Lett.*, vol. 18, no. 9, pp. 1575–1578, Sept. 2014.

[46] ——, "A mathematical framework to the computation of the error probability of downlink MIMO cellular networks by using stochastic geometry," *IEEE Trans. Commun.*, vol. 62, no. 8, pp. 2860–2879, Aug. 2014.

[47] M. D. Renzo and W. Lu, "Stochastic geometry modeling and performance evaluation of MIMO cellular networks using the equivalentin- distribution (EiD)-based approach," *IEEE Trans. Commun.*, vol. 63, no. 3, pp. 977–996, Mar. 2015.

[48] L. H. Afify, H. Elsawy, T. Y. Al-Naffouri, and M.-S. Alouini, "Unified stochastic geometry model for MIMO cellular networks with retransmissions," *IEEE Trans. Wireless Commun.*, vol. 15, no. 12, pp. 8595–8609, Dec. 2016.

[49] R. Tanbourgi, H. S. Dhillon, J. G. Andrews, and F. K. Jondral, "Dual-branch MRC receivers in the cellular downlink under spa-

tial interference correlation," in *Proc. 20th Eur. Wireless Conf.*, May 2014, pp. 13–18.
[50] M. Haenggi and R. Smarandache, "Diversity polynomials for the analysis of temporal correlations in wireless networks," *IEEE Commun. Lett.*, vol. 12, no. 11, pp. 5940–5951, Nov. 2013.
[51] Z. Chen, L. Qiu, and X. Liang, "Area spectral efficiency analysis and energy consumption minimization in multi-antenna poisson distributed networks," *IEEE Trans. Wireless Commun.*, vol. 15, no. 7, pp. 4862–4874, Jul. 2016.
[52] A. Shojaeifard, K. A. Hamdi, E. Alsusa, D. K. C. So, J. Tang, and K.-K. Wong, "Design, modeling, and performance analysis of multi-antenna heterogeneous cellular networks," *IEEE Trans. Commun.*, vol. 64, no. 7, pp. 3104–3118, Jul. 2016.
[53] T.-X. Zheng, H.-M. Wang, and M. H. Lee, "Multi-antenna transmission in downlink heterogeneous cellular networks under a threshold-based mobile association policy," *IEEE Trans. Commun.*, vol. 65, no. 1, pp. 244–256, Feb. 2017.
[54] Y. Wu, Y. Cui, and B. Clerckx, "Analysis and optimization of inter-tier interference coordination in downlink multi-antenna HetNets with offloading," *IEEE Trans. Wireless Commun.*, vol. 14, no. 12, pp. 6550–6564, Dec. 2015.
[55] R. Hernandez-Aquino, S. A. R. Zaidi, D. McLernon, and M. Ghogho, "Energy efficiency analysis of two-tier MIMO diversity schemes in Poisson cellular networks," *IEEE Trans. Commun.*, vol. 63, no. 10, pp. 3898–3911, Oct. 2015.
[56] M. N. Kulkarni, A. Ghosh, and J. G. Andrews, "A comparison of MIMO techniques in downlink millimeter wave cellular networks with hybrid beamfrming," *IEEE Transactions on Communications*, vol. 54, no. 5, pp. 1952 – 1967, May 2016.
[57] J. G. Andrews, T. Bai, M. N. Kulkarni, A. Alkhateeb, A. K. Gupta, and R. W. Heath, "Modeling and analyzing millimeter wave cellular systems," *IEEE Transactions on Communications*, vol. 65, no. 1, pp. 403–430, Jan. 2017.
[58] N. Deng, M. Haenggi, and Y. Sun, "Millimeter-wave Device-to-Device networks with heterogeneous antenna arrays," *IEEE Trans. Commun.*, vol. 66, no. 9, pp. 4271–4285, Sept. 2018.
[59] M. G. Khoshkholgh and V. C. M. Leung, "Mean delay analysis of MIMO-ZFBF multiplexing in random networks under LOS/NLOS pathloss model," *IEEE Trans. Wireless Commun.*, vol. 17, no. 8, pp. 5282–5299, Aug. 2018.
[60] ——, "Delay analysis of spatially-coded MIMO-ZFBF with re-transmissions in random networks," *to appear in IEEE Trans. Veh. Technol*, 2019.
[61] J. F. C. Kingman, *Poisson Processes*. Oxford University Press, 1993.
[62] M. Haenggi and R. K. Ganti, *Interference in large wireless networks*. NOW: Foundations and Trends in Networking, 2009.
[63] R. H. Y. Louie, M. R. McKay, and I. B. Collings, "Open-loop spatial multiplexing and diversity communications in ad hoc networks," *IEEE Transactions on Information Theory*, vol. 57, no. 1, pp. 317–344, Jan. 2011.
[64] R. Vaze and R. W. Heath Jr., "Transmission capacity of ad-hoc networks with multiple antennas using transmit stream adaptation and interference cancellation," *IEEE Transactions on Information Theory*, vol. 58, no. 2, pp. 780–792, Feb. 2012.
[65] K. R. Kumar, G. Caire, and A. L. Moustakas, "Asymptotic performance of linear receivers in MIMO fading channels," *IEEE Transactions on Information Theory*, vol. 55, no. 10, pp. 4398–4418, Oct. 2009.
[66] L. G. Ordonez, D. P. Palomar, and J. R. Fonollosa, "Ordered eigenvalues of a general class of hermitian random matrices with application to the performance analysis of MIMO systems," *IEEE Transactions on Signal Processing*, vol. 57, no. 2, pp. 672–689, Feb. 2006.
[67] H. P. Keeler, B. Blaszczyszyn, and M. K. Karray, "SINR-based k-coverage probability in cellular networks with arbitrary shadowing," in *Proc. IEEE international symposium on information theory*, 2013.
[68] B. Blaszczyszyn and H. P. Keeler, "Studying the SINR process of the typical user in poisson networks using its factorial moment measures," *IEEE Trans. Information Theory*, vol. 61, no. 12, pp. 6774–6794, Dec. 2015.
[69] K. Shen and W. Yu, "Distributed pricing-based user association for downlink heterogeneous cellular networks," *IEEE JSAC*, vol. 32, no. 6, pp. 1100–1113, June 2014.
[70] R. Sun, "Joint downlink base station association and power control for max-min fairness: Computation and complexity," *IEEE JSAC*, vol. 33, no. 6, pp. 1040 – 1054, June 2015.
[71] R. Madan, J. Borran, A. Sampath, N. Bhushan, A. Khandekar, and T. Ji, "Cell association and interference coordination in heterogeneous LTE-A cellular networks," *IEEE JSAC*, vol. 28, no. 12, pp. 1479–1489, Dec. 2010.
[72] L. P. Qian, Y. J. Zhang, Y. Wu, and J. Chen, "Joint base station association and power control via benders decompostition," *IEEE Trans. Wireless Commun.*, vol. 4, no. 12, pp. 1651–1665, Apr. 2013.
[73] M. Haenggi, "Diversity loss due to interference correlation," *IEEE Commun. Lett.*, vol. 16, no. 10, pp. 1600–1603, Oct. 2012.
[74] A. J. Goldsmith, *Wireless Communications*. Cambridge University Press, 2005.
[75] S. Zhou, Z. Wang, and G. B. Giannakis, "Quantifying the power loss when transmit beamforming relies on finite-rate feedback," *IEEE Trans. Wireless Commun.*, vol. 4, no. 4, pp. 1948–1957, July 2005.
[76] N. Jindal, "MIMO broadcast channels with finite-rate feedback," *IEEE Trans. Inf. Theory*, vol. 52, no. 11, pp. 5045–5060, Nov. 2006.
[77] M. G. Khoshkholgh and V. C. M. Leung, "Analyzing coverage probability of multitier heterogeneous networks under quantized multiuser ZF beamforming," *IEEE Trans. Veh. Technol.*, vol. 67, no. 4, pp. 3319–3338, Apr. 2018.
[78] J. Zhang, M. Kountouris, , J. G. Andrews, and R. W. Heath Jr., "Multimode transmission for the MIMO broadcast channel with imperfect channel state information," *IEEE Trans. Commun.*, vol. 59, no. 3, p. 803814, Mar. 2011.

Mohammad G. Khoshkholgh received his B.Sc. degree in Electrical Engineering from Isfahan University, Isfahan, Iran, in 2006, his M.Sc. degree in Electrical Engineering from the Tarbiat Modares University, Tehran, Iran, in 2008. He is now with the University of British Columbia. His research interests are mainly in wireless communications and networks. He is the holder of Vanier Canada Graduate Scholarship.

Keivan Navaie is with the School of Computing and Communications, Lancaster University, United Kingdom. His research interests lie in the field of mobile computing, radio resource allocation, cognitive radio networks, and cooperative communications. He is on the editorial board of the IEEE Communications Surveys & Tutorials, and IEEE Communications Letters. He has served in the technical program committee of several IEEE conferences. He is a senior member of the IEEE, an IET Fellow, and a Chartered Engineer.

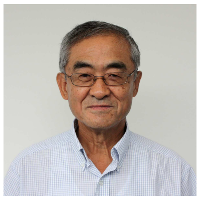

Kang G. Shin is the Kevin & Nancy O'Connor Professor of Computer Science in the Department of Electrical Engineering and Computer Science, The University of Michigan, Ann Arbor. His current research focuses on QoS-sensitive computing and networking as well as on embedded real-time and cyber-physical systems.

He has supervised the completion of 82 PhDs, and authored/coauthored about 900 technical articles (more than 330 of these are in archival journals), a textbook and more than 40 patents or invention disclosures, and received numerous best paper awards, including the Best Paper Awards from the 2011 ACM International Conference on Mobile Computing and Networking (MobiCom'11), the 2011 IEEE International Conference on Autonomic Computing, the 2010 and 2000 USENIX Annual Technical Conferences, as well as the 2003 IEEE Communications Society William R. Bennett Prize Paper Award and the 1987 Outstanding IEEE Transactions of Automatic Control Paper Award. He has also received several institutional awards.

He was a co-founder of a couple of startups and also licensed some of his technologies to industry.

Victor C. M. Leung [S75, M89, SM97, F03] received the B.A.Sc. (Hons.) degree in electrical engineering from the University of British Columbia (UBC) in 1977, and was awarded the APEBC Gold Medal as the head of the graduating class in the Faculty of Applied Science. He attended graduate school at UBC on a Canadian Natural Sciences and Engineering Research Council Postgraduate Scholarship and received the Ph.D. degree in electrical engineering in 1982. From 1981 to 1987, Dr. Leung was a Senior Member of Technical Staff and satellite system specialist at MPR Teltech Ltd., Canada. He is also serving as the Overseas Dean of the School of Information and Electronic Engineering at Zhejiang Gongshang University, China. Dr. Leung has co-authored more than 1000 journal/conference papers, 37 book chapters, and co-edited 12 book titles. Dr. Leung is a registered Professional Engineer in the Province of British Columbia, Canada.